

1 **The Determination of ClNO₂ via Thermal Dissociation-Tunable
2 Infrared Laser Direct Absorption Spectroscopy**

3
4 John W. Halfacre¹, Lewis Marden¹, Marvin D Shaw¹, Lucy J Carpenter¹, Emily Matthews², Thomas J.
5 Bannan², Hugh Coe^{2,3}, Scott C. Herndon⁴, Joseph R. Roscioli⁴, Christoph Dyroff⁴, Tara I. Yacovitch⁴,
6 Patrick R. Veres^{5*}, Michael Robinson^{5,6}, Steven S. Brown^{5,7}, Pete M. Edwards^{1,8}

7
8 ¹Wolfson Atmospheric Chemistry Laboratories, Department of Chemistry, University of York, Heslington,
9 York, YO10 5DD, UK

10 ²Department of Earth and Environmental Science, Centre for Atmospheric Science, School of Natural Sciences, The University
11 of Manchester, Manchester M13 9PL, UK

12 ³National Centre for Atmospheric Science, University of Manchester, Manchester, UK

13 ⁴Aerodyne Research, Inc., Billerica, MA, 01821, USA

14 ⁵Chemical Sciences Laboratory, National Oceanic and Atmospheric Administration, Boulder, CO, 80305, USA

15 ⁶Cooperative Institute for Research in Environmental Sciences, University of Colorado, Boulder, CO, 80305, USA

16 ⁷Department of Chemistry, University of Colorado, Boulder, CO 80309, USA

17 ⁸National Centre for Atmospheric Science, University of York, York, UK

18 *Now at National Science Foundation, National Center for Atmospheric Research, Boulder, CO, 80301, USA

19

20 Correspondence to: John Halfacre (john.halfacre@york.ac.uk), Pete Edwards (pete.edwards@york.ac.uk)

21 **Abstract.** Nitryl chloride (ClNO₂) is a reservoir species of chlorine atoms and nitrogen oxides, both of which play important
22 roles in atmospheric chemistry. To date, all ambient ClNO₂ observations have been obtained by chemical ionization mass
23 spectrometry (CIMS). In this work, Thermal Dissociation Tunable Infrared Laser Differential Absorption Spectrometer (TD-
24 TILDAS) is shown to be a viable method for quantifying ClNO₂ in laboratory and field settings. This technique relies on the
25 thermal dissociation of ClNO₂ to create chlorine radicals, which undergo fast reactions with hydrocarbons to produce hydrogen
26 chloride (HCl) that is detectable by the TILDAS instrument. Complete quantitative conversion of ClNO₂ to HCl was achieved
27 at temperatures > 400°C, achieving 1 Hz measurement precision of 11 ± 1 pptv (3σ limits of detection of 34 ± 2 pptv) during
28 laboratory comparisons with other ClNO₂ detection methods. After blank- and line loss-corrections, method accuracy is
29 estimated to be within ± 5%. Performance metrics of TD-TILDAS during ambient sampling were a 1 Hz precision of 19 ± 1
30 pptv and 3σ limits of detection of 57 ± 3 pptv), which is directly comparable to previously reported ClNO₂ detection by
31 quadrupole CIMS. Thus, TD-TILDAS can provide an alternative analytical approach for a direct measurement of ClNO₂ that
32 can complement existing datasets and future studies. The quantitative nature of TD-TILDAS also makes it a potentially useful
33 tool for the calibration of CIMS instruments. However, interpretation of ambient data may be potentially complicated by
34 potential interference from unaccounted-for sources of thermolabile chlorine, such as ClNO, chloramines, and
35 organochlorides.

36 **1 Introduction**

37 Nitryl chloride (ClNO_2) is an important nighttime reservoir of two highly reactive atmospheric species: atomic Cl and NO_2 .
 38 Atomic Cl radicals play multifaceted roles in oxidation chemistry throughout the boundary layer (Simpson et al., 2015),
 39 including hydrocarbon oxidation (Atkinson et al., 2006a, and references therein), ozone production and destruction (Halfacre
 40 and Simpson, 2022; Liao et al., 2014; Sarwar et al., 2012, 2014; Simon et al., 2009; Wang et al., 2016), and mercury depletion
 41 (Driscoll et al., 2013). However, the quantitative magnitude to which they affect these processes remains an open question. On
 42 the other hand, NO_2 is one of the principal components of photochemical smog and the major anthropogenic precursor for
 43 ozone production. Accounting for all sources of NO_2 is therefore important for accurately informing chemical and air quality
 44 models.

45 The first in situ observation of ambient ClNO_2 was reported by Osthoff et al. (2008) utilising chemical ionization
 46 mass spectrometry (CIMS) in the polluted marine boundary layer. CIMS has since been used in a multitude of studies for
 47 additional ClNO_2 observations worldwide, including North America (Jaeglé et al., 2018; Lee et al., 2018a, b; Mielke et al.,
 48 2011; Riedel et al., 2012, 2013; Thornton et al., 2010; Wagner et al., 2013; Young et al., 2012), Europe (Bannan et al., 2015;
 49 Phillips et al., 2012; Sommariva et al., 2018; Tan et al., 2022), Asia (Le Breton et al., 2018; Liu et al., 2017; Tham et al., 2016,
 50 2018; Wang et al., 2022, 2016, 2017; Xia et al., 2020; Ye et al., 2021; Yu et al., 2020; Zhou et al., 2018), in the presence of
 51 snow/ice (Kercher et al., 2009; McNamara et al., 2020), and in indoor air quality studies (Moravek et al., 2022). Limits of
 52 detection are often reported at 10^0 pptv under 25–30 s averaging times, (Bannan et al., 2015; Kercher et al., 2009; McNamara
 53 et al., 2020; Mielke et al., 2011), and has been recently reported at sub-pptv for 1 s measurements (Decker et al., 2024). Typical
 54 observed mixing ratios range from 10^1 – 10^3 pptv, with the highest levels observed in coastal polluted regions, where sources
 55 of nitrogen oxides and Cl-rich aerosols are plentiful (Wang et al., 2019, 2021, and references therein).

56 While CIMS is a highly effective technique, ClNO_2 quantitation involves non-trivial calibration work. A laboratory
 57 source of ClNO_2 may be readily generated by flowing a known amount of N_2O_5 across a Cl^- -containing salt bed (or Cl_2 across
 58 NO_2^- -containing salt bed), but its quantitation assumes unit conversion out of the salt bed (e.g., Osthoff et al., 2008) or requires
 59 additional equipment to observe ClNO_2 thermal dissociation products, such as a N_2O_5 thermal dissociation-cavity ring down
 60 spectrometer (TR-CRDS) (Thaler et al., 2011) or a cavity attenuated phase shift spectrometer (CAPS) (e.g., Tan et al., 2022).
 61 Further, I based CIMS demonstrates variable sensitivities based on the temperature and relative humidity of the ion-molecule
 62 reactor, thereby requiring substantial laboratory work to develop humidity- and temperature-dependent calibration factors (Lee
 63 et al., 2014; Robinson et al., 2022). Thus, there is an opportunity to innovate a method that can detect ClNO_2 directly without
 64 the need for supplemental instrumentation.

65 The advantages of optical methods include analyte specificity and near absolute detection, utilizing well-defined
 66 physical absorption properties, and requiring only infrequent calibrations or method validation procedures. Thaler et al. (2011)
 67 previously used a TR-CRDS system (tuned for the detection of peroxyacetyl nitrates) to detect ClNO_2 as NO_2 by absorption at
 68 405 nm under laboratory conditions, achieving CIMS-competitive metrics (e.g., reported 20 pptv limit of detection for 1 minute
 69 averaging). This was achieved by flowing sample air through both an unheated reference pathway and a heated (450°C) sample
 70 pathway, under which ClNO_2 would thermally dissociate into Cl radicals and NO_2 (Reaction R1).



74 The difference in observed NO_2 signal between the two channels provided a quantitative ClNO_2 measurement. However, its
 75 use for conducting field measurements was reported to be limited, as the thermal degradation of alkyl nitrates (i.e., PAN) into
 76 NO_2 cannot be distinguished from NO_2 originating from ClNO_2 due to overlapping thermal dissociation profiles.

77 For this same thermal-dissociation setup, product chlorine radicals will react quickly (e.g., Cl radical lifetime of 0.2
 78 s for typical CH_4 mixing ratios of 2 ppmv and $k_{298} = 1 \times 10^{-13} \text{ cm}^3 \text{ molecule}^{-1} \text{ s}^{-1}$ (Bryukov et al., 2002)) with ambient
 79 hydrocarbons (e.g., methane) to form hydrogen chloride (HCl), which is a stable reservoir species for reactive chlorine
 80 (Reaction R2).



84 Several optical methods for the high-frequency and precise detection of HCl have recently been reported that overcome
 85 historical challenges with its sampling (Furlani et al., 2021; Hagen et al., 2014; Halfacre et al., 2023; Wilkerson et al., 2021),
 86 making them attractive candidates for an alternative thermal dissociation approach for the detection of ClNO_2 . In this work,
 87 we demonstrate the coupling of a thermal dissociation furnace to HCl -TILDAS (TD-TILDAS) for quantitative detection of
 88 ClNO_2 as HCl . Compared with CIMS, TD-TILDAS is a lower time-cost method for determining ClNO_2 mixing ratios,
 89 involving less experimental calibration work and simpler data processing as a direct method.

90 **2 Methods**

91 **2.1 ClNO_2 Generation**

92 ClNO_2 was synthesized by flowing Cl_2 across a nitrite-rich slurry, as described by Thaler et al. (2011) and shown by Reaction
 93 R3.



97 However, it is believed the ClNO_2 , once produced, may react further by dissolving into the water, hydrolyzing, and producing
 98 nitronium and chloride ions (R4) (Frenzel et al., 1998).



102 The nitronium ion can then react with NO_2^- to produce N_2O_4 , which exists in equilibrium with NO_2 (R5).



106 As detailed by Thaler et al. (2011), this chemistry can be mitigated by minimizing the residence time of ClNO_2 in the reaction
 107 vessel and, to a lesser extent, by increasing the Cl^- content of the slurry to encourage the equilibrium in R4 towards ClNO_2 .
 108 Therefore, we composed our slurry using sodium chloride (>99.5% pure, BioXtra, Sigma Aldrich product no S7653-5KG,
 109 USA) and sodium nitrite (99%, extra pure, Acros Organics Code 196620010, Belgium) at a mole ratio of 100:1 $\text{Cl}^-:\text{NO}_2^-$,
 110 wetting with 18MΩ deionized water (Millipore). The slurry was housed in ~10 cm of 1.25 cm diameter PFA tubing. Varied
 111 flow rates ($0.5\text{--}5 \text{ mL min}^{-1}$) of 10 ppmv Cl_2 (diluted in nitrogen, BOC product no. 150916-AV-B, United Kingdom) were
 112 injected into a dilution flow (ranging from $200\text{--}2499.5 \text{ mL min}^{-1}$) of NO_x -scrubbed compressed air (using trap composed of

113 50% Sofnofil (Molecular Products Ltd., Essex, United Kingdom) and 50% activated carbon) that was subsequently passed
 114 over the slurry, generating ClNO_2 . A portion of the dilution flow was directed into a bubbler containing $18\text{M}\Omega$ deionized water
 115 prior to entering the slurry to maintain a humid environment and prevent the slurry from drying out. A schematic diagram of
 116 this setup is presented in Fig. 1a.

117 **2.2 TD-TILDAS**

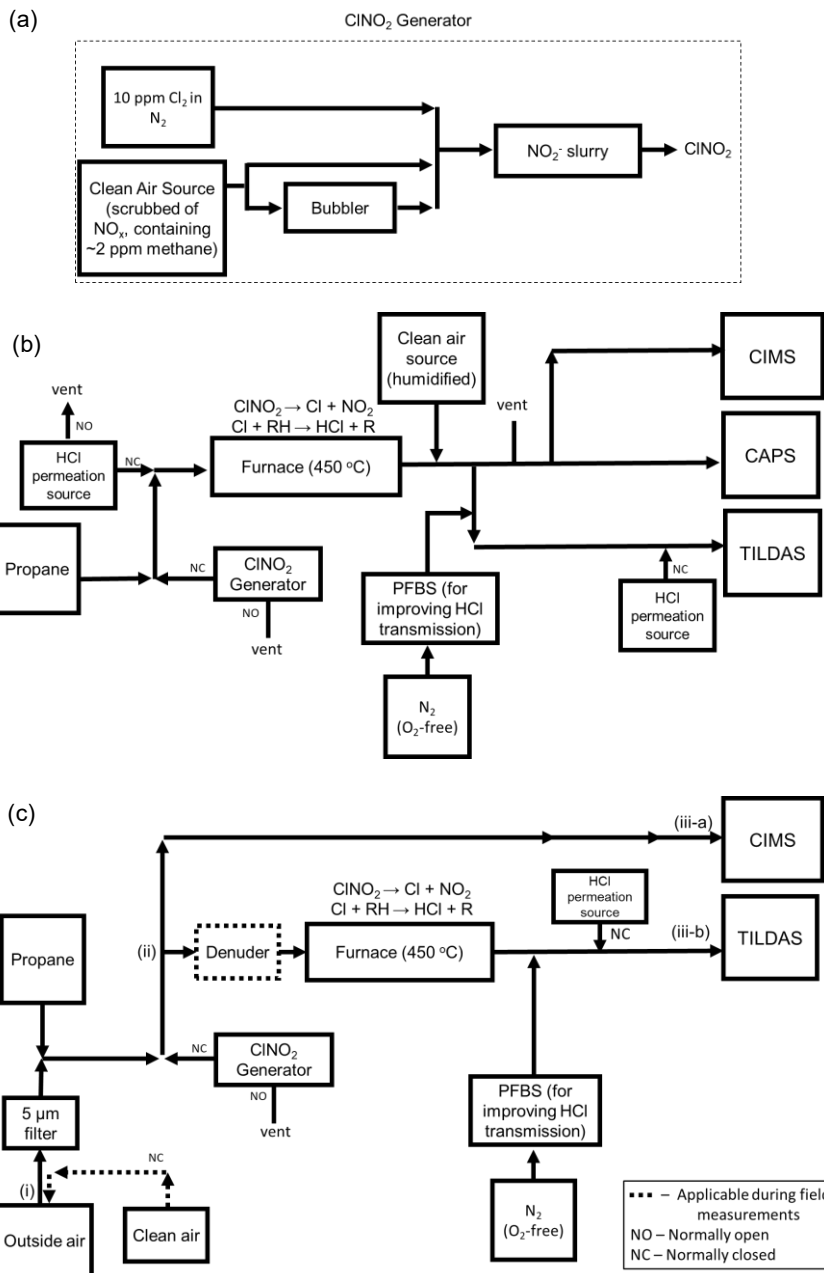
118 The TILDAS instrument and operation technique have been well-described previously (McManus et al., 2011, 2015). HCl-
 119 TILDAS was developed by Aerodyne Research, Inc. and characterized by Halfacre et al. (2023). Briefly, air is sampled at 3.0
 120 L min^{-1} through a heated (50°C) quartz “inertial inlet,” which is a type of virtual impactor used to remove particles $>300\text{ nm}$
 121 from the sample matrix. Sample air continues its flow through 3 m of heated (50°C) tubing into the Herriott cell (204 m
 122 pathlength) inside the TILDAS. HCl is then detected via a mid-IR inter-band cascade laser that probes the strong $\text{R}(1) \text{H}^3\text{Cl}$
 123 absorption line at $2925.89645\text{ cm}^{-1}$ within the (1-0) rovibrational absorption band (Guelachvili et al., 1981).

124 Nitryl chloride was converted to HCl for detection by TILDAS via thermal dissociation and the subsequent reaction of Cl
 125 radicals with hydrocarbons, namely methane (Reactions R1-R2) (Thaler et al., 2011). While modelling results predicted
 126 ambient mixing ratios of methane (~2 ppmv) are sufficient for achieving unit conversion of 1 ppbv ClNO_2 to HCl (Sect. 3.1),
 127 The sample flow was additionally spiked with propane (BOC Limited, product no. 34-A), to a mixing ratio of 5 ppmv to both
 128 ensure reaction completeness and outcompete Cl wall losses, as the rate constant for the reaction between Cl and propane is 3
 129 orders of magnitude faster than with methane (Atkinson et al., 2006a). Next, the sample was directed to a 90 cm length of
 130 quartz tubing (9.5 mm OD, 7.5 mm ID) housed within a furnace (Carbolite Gero TS1 12/60/450) upstream of the inertial inlet.
 131 Sixty centimetres of this tubing is held within the heated region of the furnace, resulting in a residence time of $\sim 500\text{ ms}$ under
 132 a flow rate of 3 L min^{-1} . The internal temperature of the furnace is monitored using the furnace's inbuilt temperature sensors
 133 and logged using the furnace software. To mitigate HCl surface interactions after ClNO_2 -conversion, perfluorobutane-1-
 134 sulfonic acid (PFBS; Merck, product no. 562629, United Kingdom) vapor was introduced just after the furnace to actively
 135 passivate tubing and inlet surfaces, improve improving HCl transmission to the TILDAS inlet by 1) displacing HCl sorbed to
 136 surfaces and 2) increasing the non-polar character of surfaces by presenting a fluorinated chain to passing analytes (Halfacre
 137 et al., 2023; Roscioli et al., 2016). As detailed by Halfacre et al. (2023), a flow ($50\text{--}75\text{ mL min}^{-1}$) of oxygen-free nitrogen was
 138 flowed into the headspace of a Teflon bubbler containing 5 g of PFBS, thereby flushing the PFBS vapor into the sample line.
 139 A schematic diagram of this setup is presented in Fig. 1b.

140 The major sources of uncertainty with using TD-TILDAS to detect ClNO_2 include the degree of ClNO_2 conversion
 141 to HCl, instrument noise, background drifts, and potential line losses of HCl. Confirmation of the unit conversion of ClNO_2 to
 142 HCl was confirmed by modelling and laboratory experiments (see Sects. 3.1 and 3.2). Instrument noise and background drifts
 143 were assessed regularly from blanks. For laboratory experiments, blanks were performed by sampling the ClNO_2 standard
 144 (Sect. 2.1) diluted in NO_x -scrubbed compressed air through the unheated furnace. This dilution air was generated using an air
 145 compressor and dehumidifying system (dew point approximately -60°C , absolute water vapor concentration $\sim 0.01\%$). To
 146 vary sample humidity, carrier gas flow was split such that varied amounts were passed through a bubbler containing deionized
 147 water. Concerning line losses of HCl, the only source of HCl will be from ClNO_2 conversion during laboratory experiments,
 148 and therefore line losses were assessed between the furnace and the inertial inlet. As detailed in Fig. 1b, 30 mL min^{-1} of flow
 149 from a homemade HCl permeation source (Furlani et al., 2021; Halfacre et al., 2023) was injected alternately before the
 150 furnace and just before the inertial inlet to determine loss of HCl over this region. So long as unit conversion of ClNO_2 to HCl
 151 can be confirmed and blank / line losses are corrected, this method will be as accurate as the TILDAS is for detecting HCl,

152 which was previously found to be within the 5% tolerance of a commercial HCl cylinder with a certified concentration
153 (Halfacre et al., 2023).

154 For ambient sampling (Fig. 1c), an additional 5m of 1.25 cm OD PTFA Teflon was added before the tee that splits
155 the CIMS and TILDAS flow paths to sample outside air. A 5 μm PFA Teflon filter was also installed to collect particulates,
156 reducing the potential for HCl displacement through thermodynamic partitioning of particulate Cl⁻ that would otherwise enter
157 the heated furnace (Huffman et al., 2009). This Teflon filter was not found to affect the observed mixing ratio of our ClNO₂
158 standard in measurement comparisons with and without the filter. However, the collection of particulates on the filter could
159 enable heterogenous chemistry with passing N₂O₅ plumes that may produce corresponding ClNO₂ plumes that are not reflective
160 of ambient chemistry, and so frequent replacement of these filters is necessary (e.g., daily). Blank air was generated by
161 pumping ambient air through a 50% activated carbon / 50% Sofnofil scrubber, which was found to effectively remove ClNO₂
162 from the sample stream. The pump (KNF model N035.1.2AN.18) was able to overblow the sample inlet at a flow rate of ~25
163 L min⁻¹. This approach is favoured over the use of synthetic cylinder air as significant changes in sample humidity can result
164 in release of HCl from surfaces (Halfacre et al., 2023). Blanks were performed for 10 minutes every 30 minutes to ensure the
165 instrument had enough time to respond and adjust to a stable background value. Additionally, ambient measurements will
166 include HCl, which would act as an interference for ClNO₂ observations. To obviate this, a denuder (coating of 2% Na₂CO₃
167 and 2% glycerol dissolved in 50% water and 50% methanol) was installed before the furnace to selectively remove acidic
168 gases (e.g., HCl, HNO₃) that may influence quantitation. Using the denuder for this purpose was While effective for this
169 purposefound to be effective for at least one-week periods, after which it was generally replaced to avoid coating exhaustion.
170 the-The denuder was also found to affect ClNO₂ throughput on shorter term timescales (e.g., daily), with a freshly coated
171 denuder causing as much as 55% loss of the ClNO₂ standard mixing ratio. This was determined by calculating the percent
172 difference when sampling the ClNO₂ standard both through and bypassing the denuder. As suchBecause ClNO₂ additions
173 during ambient sampling will always be added through the denuder, it was important that the ClNO₂ standard (Sect. 2.1) was
174 sampled in dry air before and after overnight experiments to quantify estimate how this loss process evolved over the course
175 of an experiment such that data could be corrected using the percent difference term. -Periodic additions of HCl standard were
176 also performed to assess line losses of HCl after conversion in the furnace. In contrast to the laboratory experiment
177 configuration, permeation source HCl in blank air was only injected just downstream of the furnace mid-experiment to reduce
178 exposure of unpassivated sampling surfaces to HCl. Losses were assessed by comparing this observed HCl injection value to
179 pre- and post-experiment injections over dry compressed air. Injections of HCl and ClNO₂ standards was controlled using 3-
180 way Teflon solenoid valves (MasterFlex Model no. 01540-18, Cole Parmer, United Kingdom).



181
 182 Figure 1 Experimental schematic diagrams for (a) generating CINO₂, b) laboratory comparison measurements between CIMS,
 183 TILDAS, and CAPS NO₂, and (b,c) calibration/field sampling between CIMS and TILDAS. Note that "NO" stands for "normally
 184 open" and "NC" stands for "normally closed" in reference to solenoid valves that control the flow direction for these items. For (c),
 185 the approximate distance between point (i) and (ii) is 5 m, from (ii) to (iii-a) is 1.5 m, and from (ii) to (iii-b) is 2 m.

186 **2.3 Supporting Instrumentation**

187 To confirm the efficacy of TD-TILDAS as a valid quantitative method for ClNO_2 detection, testing was performed
188 simultaneously with a Cavity Attenuated Phase Shift (CAPS) NO_2 instrument (Sect. 2.3.1) and Time of Flight-Chemical
189 Ionization Mass Spectrometer (Sect. 2.3.2), both of which have previously reported as ClNO_2 detection methods.

190 **2.3.1 Cavity Attenuated Phase Shift (CAPS) NO_2**

191 ClNO_2 mixing ratios observed by the TILDAS were confirmed via simultaneous detection of the NO_2 product of ClNO_2 thermal
192 dissociation using a commercial Cavity Attenuated Phase Shift NO_2 detector (Teledyne T500U CAPS). Briefly, emission from
193 a LED (emission centred around 425 nm) is reflected across two spherical mirrors and absorbed by NO_2 in the optical cell.
194 This difference in light is detected by a photodiode and quantified based on its absorbance via the Beer-Lambert Law. The
195 instrument was calibrated using gas-phase titration of NO by O_3 to produce varied concentrations of NO_2 . A 1 ppm NO in
196 nitrogen cylinder (certified 982 ppb, NPL) was used to verify the concentration of NO in a 25 ppm NO in nitrogen working
197 standard (BOC). A multigas blender (Environics S6100) was used to generate a range of O_3 concentrations (range 0-130 ppbv)
198 for titrating some of the NO (NO in excess, 200 ppbv) into NO_2 , and the decrease in the NO concentrations was measured
199 using a calibrated NO_x instrument (Teledyne API Chemiluminescence T200). The NO_2 introduced to the CAPS instrument is
200 thus the sum of the drop of NO from the added ozone and the NO_2 already present in the working standard. The T200 NO_x
201 instrument was also used to measure ambient air alongside the CAPS (range 0-25 ppbv), and these data are presented in Fig.
202 A1. Additionally, the Teledyne T500U includes an internal drying assembly and has a manufacturer recommended humidity
203 range of 0 – 95%.

204 **2.3.2 Time of Flight Chemical Ionisation Mass Spectrometry (CIMS)**

205 ClNO_2 was additionally detected using a VOCUS high-resolution chemical ionization time-of-flight CIMS (Tofwerk,
206 Switzerland) with a VOCUS AIM reactor and using iodide (I^-) as a reagent ion gas. A complete description of this instrument
207 and its operational principles are described in detail by Riva et al. (2024). Briefly, sample gas is drawn into the sampling inlet
208 and pulled through a critical orifice (0.475 mm) and PFA Teflon sample flow guide into a conical ion-molecule reactor (IMR)
209 at a flow rate of 1.8 L min⁻¹. The IMR was held at a constant pressure of 50 mbar using a vacuum pump (IDP3, Agilent
210 Technologies) and temperature controlled to 50 °C. The reagent ion source was a permeation tube containing trace amounts of
211 CH_3I dissolved in benzene (Tofwerk). Ultra-high purity, oxygen-free N_2 gas (generated by flowing compressed air through
212 gas with a commercial N_2 generator, Infinity NM32L, Peak Scientific Instruments, UK) is continually flowed over the
213 permeation tube to flush the gaseous CH_3I /benzene mixture into a compact vacuum ultraviolet ion source (VUV). Within the
214 VUV, UV light emitted from a Kr lamp (116.486 nm and 123.582 nm) is absorbed by benzene, generating low energy
215 photoelectrons that can react with CH_3I to produce I^- (Ji et al., 2020). The I^- reacts with analytes for approximately 30 ms
216 before being drawn through another critical orifice where the sample travels through four differentially pumped chambers
217 before reaching the drift region of the ToF-CIMS. Ions in the ToF chamber are extracted and converted into mass spectra via
218 an MCP detector with a preamplifier over a mass range of 7-510 Th. The extracted packets are averaged over a period of 1
219 second and the resolution of the instrument is \approx 5000. Data was collected at a rate of 1 Hz. Data averaging, mass calibration,
220 peak assignment, peak fitting and peak integration are all performed using the software package Tofware (version 4.0.0,
221 TOFWERK) used in Igor Pro 9 software (Wavemetrics). Peak fitting focused on $\text{I}^{35}\text{ClNO}_2^-$ (m/z 207.8668) and $\text{I}^{37}\text{ClNO}_2^-$ (m/z
222 209.8638), and isotope abundances were manually confirmed to be \sim 1:0.32, based on the natural abundance of chlorine
223 isotopes. CIMS signals were normalized against the sum of the total number of reagent ions, which is equivalent to $\text{I}^- + \text{I}(\text{H}_2\text{O})^-$

224 . Additionally, as the CIMS sensitivity to ClNO₂ varies with humidity in the ion-molecule reactor region, we define an
225 additional term equal to ratio of the iodide water cluster (I(H₂O)[·]) to the reagent ion sum (I[·] + I(H₂O)[·]), hereafter referred to as
226 the Iodide Water Ratio (IWR). Instrument backgrounds were assessed using air scrubbed of ClNO₂, as described in Sect. 2.2.

227 **2.4 Data Analysis**

228 Data analysis was conducted using the R language for statistical computing (R Core Team, 2021). Linear regressions were
229 calculated using the York method (Cantrell, 2008) when possible so as to incorporate uncertainties in compared variables.

230 **2.5 Chemical Modelling**

231 The 0-D box model Kintecus (Ianni, 2003, 2022) was used to [explore the gas phase chemistry occurring in the heated furnace](#)
232 [to predict the timescales for of the thermal-dissociation of ClNO₂ and the subsequent formation of HCl after reaction with](#)
233 [hydrocarbons \(Reaction R2-₂\), as well as. The only hydrocarbon included in these model experiments was methane. The model](#)
234 [was also used to identify potential interferences that could prevent unit conversion of ClNO₂ to HCl. The results of the model](#)
235 [were used to guide the experimental set-up. The modelled species, reaction list, tested interferences \(including ClNO and](#)
236 [alkenes\), and initial concentrations are included in the Appendix \(Tables A1-A3\). Reaction kinetics were sourced from the](#)
237 [NIST Chemical Kinetics Database and IUPAC Evaluated Kinetic Data websites \(Manion et al., 2015; Wallington et al., 2021\),](#)
238 [and primary literature references are listed next to each reaction. No chemical species were held constant or were otherwise](#)
239 [constrained outside of initial concentrations. The model integration time was set to 1 ms, and the entire simulation was set to](#)
240 [last 150 ms. The model initiated with a temperature of 25 °C \(held for 10 ms\) before increasing to 450 °C over the course of](#)
241 [22 ms. The temperature was held at 450 °C for 40 ms, before gradually decaying back to 25 °C over 70 ms.](#)

242 **3 Results & Discussion**

243 **3.1 Modelling TD Chemistry**

244 Box model simulations predicted the rapid, virtually unit conversion of ClNO₂ to HCl after increasing temperature to 450 °C
245 (Fig. 2) [under the model conditions outlined in Tables A1-A3](#). Ninety percent conversion was calculated to occur within 23
246 ms from a starting ClNO₂ concentration of 2.46×10^{10} molecules cm⁻³ (1 ppbv at 25 °C), and ambient mixing ratios of methane
247 (i.e., 2 ppmv at 25 °C) were found to be sufficient for facilitating this chemistry. While Cl-mediated hydrocarbon oxidation
248 was shown to produce a modest enhancement of hydroxyl radical concentrations (Fig. 2b), it was not enough to compete
249 meaningfully with Cl to mitigate or retard Reaction R1. Similarly, an initial O₃ concentration of 9.84×10^{11} molecules cm⁻³
250 (40 ppbv at 25 °C) did not significantly inhibit the desired chemistry by the direct reaction of O₃ with Cl radicals.

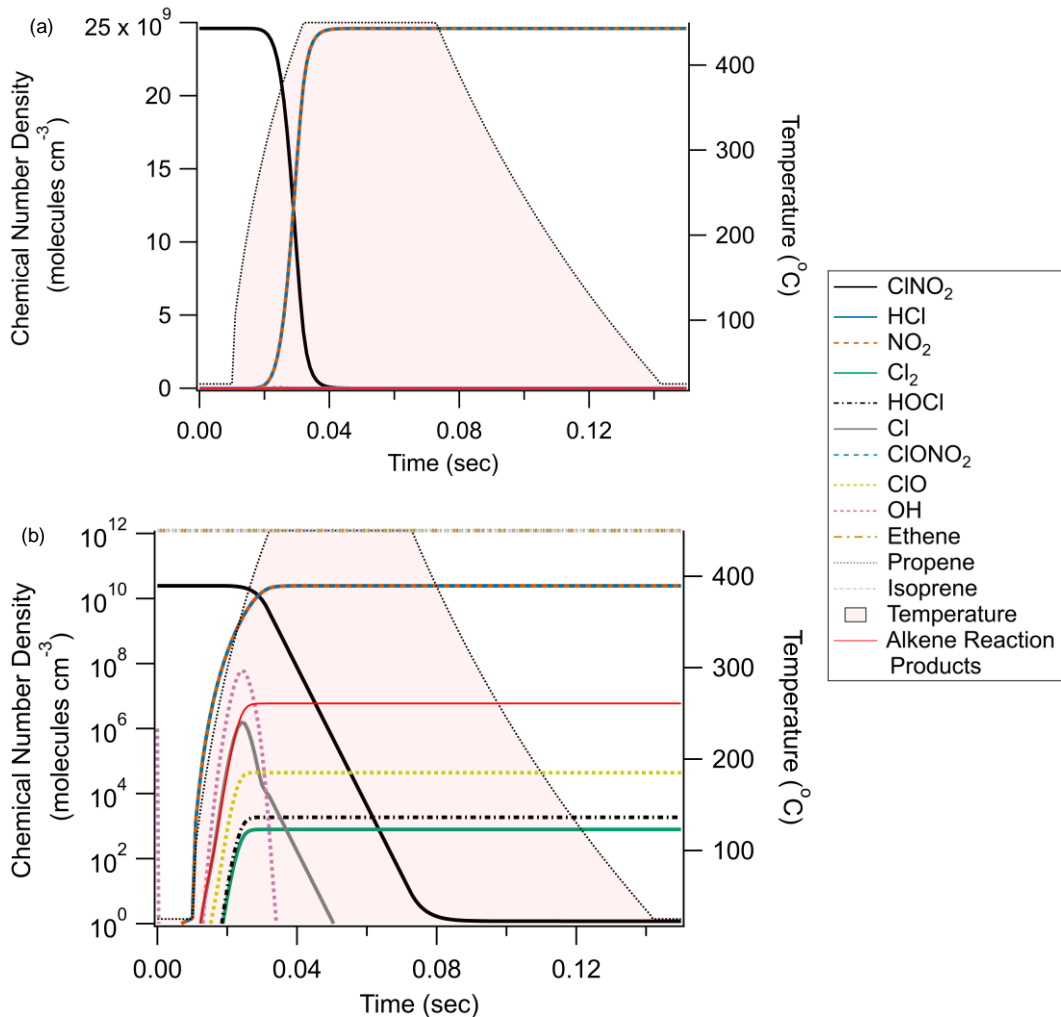


Figure 2: Chemical modelling results of the thermal dissociation of CINO₂ and its subsequent conversion to HCl. Panel A presents results on a linear y-axis, while Panel B features the same data on a logarithmic y-axis. Note that ethene, propene, and isoprene are off-scale in Panel A (1.23×10^{12} molecules cm⁻³ / ~50 ppbv) to better display the relationships between CINO₂, HCl, and NO₂, and are shown to remain constant in Panel B.

Concerning potential interferents, Cl can add to double bonds found on alkenes without producing HCl. Reactions with ethene, propene, and isoprene were included in the model at 1.23×10^{12} molecules cm⁻³ (50 ppbv at 25° C) each and were found to produce approximately 1×10^6 molecules cm⁻³ of non-HCl product, which is 4 orders of magnitude less than the HCl converted from CINO₂. As these mixing ratios of alkenes are larger than those typically found in real world environments (e.g.,

258 Budisulistiorini et al., 2015; Hellén et al., 2024; Tripathi et al., 2021, it is therefore unlikely alkenes will cause meaningful
 259 interference for ClNO_2 quantification.

260 ClNO_2 was predicted to be the only known source of inorganic chlorine reservoir to thermally dissociate at 450 °C.
 261 This is consistent with the relative bond dissociation energies found for ClNO_2 (142 kJ mol⁻¹) relative to the various other
 262 forms of inorganic chlorine simulated ($\text{Cl-NO}_2 < \text{Cl-Cl} < \text{Cl-O} < \text{Cl-R} < \text{Cl-H}$) (Darwent, 1970). Finally, p
Production of other
263 inorganic chlorine compounds (e.g., Cl_2 , HOCl , ClONO_2 , or reformation of ClNO_2) was orders of magnitude less than the
264 resulting HCl and is therefore not believed to influence HCl production. Even so, there remain potential inorganic chlorine
265 species that may still act as interferences in this method. Nitrosyl chloride (CINO) has been previously predicted by modelling
266 to exist at ppbv-level mixing ratios in polluted marine environments and could be an efficient Cl-atom source (Raff et al.,
267 2009). Indeed, 1 ppbv (2.46×10^{10} molecules cm⁻³) of CINO was found to partially thermally dissociate in our Kintecus model
268 (bond dissociation energy of 159 kJ mol⁻¹) and generate additional HCl, as well as NO that was gradually converted to NO_2
269 (Fig. A2). On the addition of heat, CINO decreased by 40% while HCl increased by an equivalent amount (in addition to the
270 2.46×10^{10} molecules cm⁻³ generated by ClNO_2 thermal dissociation). While we are unaware of any field measurements that
271 have confirmed the presence of CINO in the boundary layer to date, it appears likely this method would be sensitive to
272 interference from CINO if/where its presence is confirmed.

273 Finally, production of other inorganic chlorine compounds (e.g., Cl_2 , HOCl , ClONO_2 , or reformation of ClNO_2) was
274 orders of magnitude less than the resulting HCl and is therefore not believed to influence HCl production. Additionally, O
275 one notable class of compounds that could not be simulated were chloramines, which have recently received increased attention as
276 relevant daytime sources of Cl atoms (A. Angelucci et al., 2023; Wang et al., 2023). Their largest known anthropogenic sources
277 include water disinfection processes, swimming pools, and cleaning products. Trichloramine, dichloramine, and
278 monochloramine have reported bond dissociation energies of 381, 280, 251 kJ mol⁻¹, respectively (Darwent, 1970) (ClNO_2
279 bond dissociation energy = 142 kJ mol⁻¹), and so would not be expected to produce free Cl radicals in the temperature range
280 simulated herein if its thermochemistry is consistent with the above bond dissociation energy trend. However, to the authors'
281 knowledge no information is available regarding ~~its~~ their thermal stability in the gas phase at atmospherically relevant
282 conditions, and this potential source of positive interference for our proposed method cannot be discounted via the model at
283 this time. Similarly, prevalent organochlorides, such as methyl chloride (CH_3Cl), dichloromethane (CH_2Cl_2), chloroform
284 (CHCl_3), and carbon tetrachloride (CCl_4) could cause positive interference if they dissociate and produce Cl atoms in the
285 furnace (World Meteorological Organization, 2022). Global average mixing ratios for CH_3Cl , CH_2Cl_2 , CHCl_3 , and CCl_4 were
286 ~ 550 pptv, ~ 40 pptv, 9 pptv, and 77 pptv, respectively, during 2020. Appropriate thermal dissociation kinetic parameters
287 could not be sourced for the conditions used herein (i.e., temperatures ≤ 450 °C), and so these compounds could not be properly
288 simulated by the Kintecus model. Similarly to the chloramines, the bond dissociation energies are much higher than other
289 compounds simulated (339, 310, 346, 293 kJ mol⁻¹ for CH_3Cl , CH_2Cl_2 , CHCl_3 , and CCl_4 , respectively) (Darwent, 1970;
290 Weissman and Benson, 1983)).

291 3.2 Laboratory Characterization of TD-TILDAS

292 For laboratory characterization, a stable source of ClNO_2 was generated (Sect. 2.1) for assessing TD-TILDAS
 293 performance in comparison with other established ClNO_2 sampling techniques, including CAPS NO_2 and CIMS (Sect. 2.3).
 294 One key change between model simulations and this experimental setup is the inclusion of propane to the sample stream
 295 (estimated mixing ratio of 5 ppmv within the heated section of sample configuration). While the model predicted the pertinent
 296 chemistry will occur in ~23 ms using only ambient methane as the hydrocarbon (Sect. 3.1) and the residence time in the heated
 297 furnace is ~500 ms, adding propane ensures complete conversion of ClNO_2 to HCl and ensures wall losses are negligible, as

298 Cl radicals react with propane approximately 3 orders of magnitude faster than with methane (Atkinson et al., 2006a). The fact
 299 that no additional HCl signal was observed on addition of propane at varying levels (not shown) supports our calculations that
 300 unit conversion is achieved and competitive loss of Cl radicals to walls is negligible.

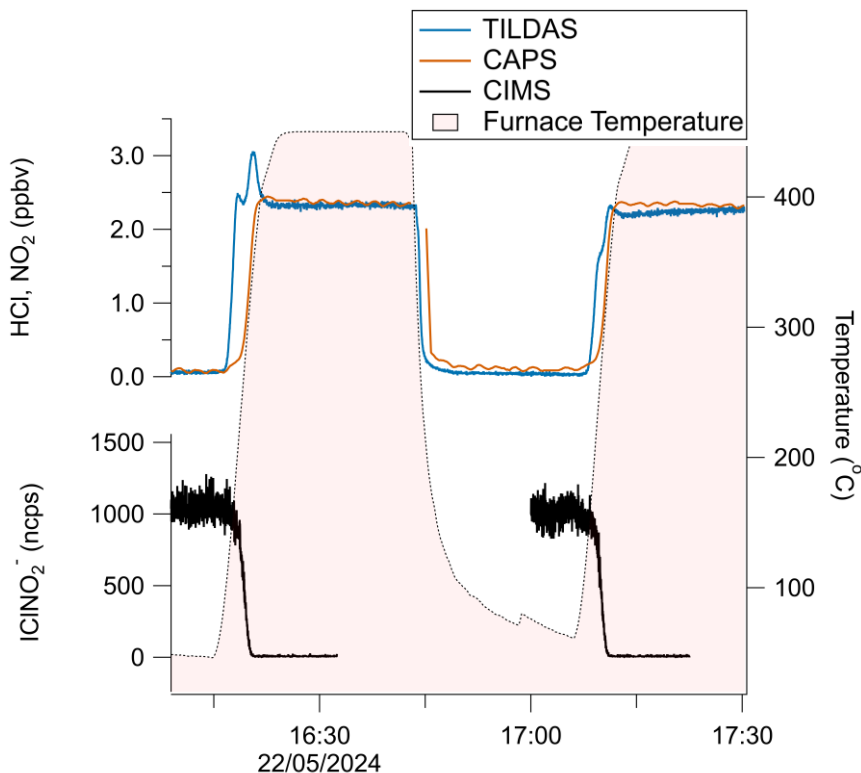
301 A schematic diagram of these experiments is shown in Fig. 1a. Figure 3 represents a typical comparison experiment
 302 in which ClNO_2 was sampled by all three instruments simultaneously. First, ClNO_2 was introduced into the flow stream with
 303 the furnace unheated, yielding a positive CIMS signal for IClNO_2^- (~1100 ncps for the example in Fig. 3), while TILDAS HCl
 304 and CAPS NO_2 mixing ratios remained at background levels. As the furnace temperature approached 450 °C, Reactions R1-
 305 R2 began to occur. HCl and NO_2 mixing ratios rose, plateauing at similar values (~2.2 ppbv in Fig. 3) while IClNO_2^- decreased
 306 to the instrument baseline, implying both Reactions R1-R2 proceeded to completion. Signals returned to their original positions
 307 once the furnace was allowed to cool back to room temperature (e.g., from 16:45 in Fig. 3). Note that HCl signal spike during
 308 the furnace's temperature ramp was seen consistently across experiments, and was most likely caused by a shift in HCl
 309 molecule partitioning between the surface of the quartz tubing toward the gas phase (Halfacre et al., 2023). Allan-Werle
 310 deviation calculations demonstrate favourable performance metrics for TILDAS while sampling ClNO_2 , with 1 Hz precision
 311 of 11.8 pptv, and as good as 1.2 pptv with an integration time of 96 seconds (Fig. 4).

312 A summary of comparison experiments across varied humidities is presented in Fig. 5. The changes in HCl as
 313 observed by TILDAS correlated strongly with the changes in NO_2 observed by the CAPS instrument (Pearson correlation
 314 coefficients of 0.999, 0.997, and 0.987 for relative humidities of 11%, 44%, and 66%, respectively). However, the slopes were
 315 consistently less than unity (0.95 ± 0.01 , 0.93 ± 0.02 , and 0.91 ± 0.02 at 11%, 44%, and 66%, respectively), indicating observed
 316 HCl mixing ratios were less than corresponding NO_2 mixing ratios. One potential explanation for this could be loss of Cl
 317 radicals loss in the furnace, but we do not believe this to be the case (as detailed above). While physical losses of HCl to
 318 sampling lines would not be unexpected as HCl has a high affinity for sorbing to physical surfaces, experiments were designed
 319 to minimize these interactions, and line loss experiments were performed to quantify any losses observed at tested humidities.
 320 Experimentally, a small flow (50-75 mL min⁻¹) of PFBS vapour was injected into the TILDAS sampling line downstream of
 321 the furnace to reduce HCl affinity for surfaces (Sect. 2.2) (Note that PFBS was not introduced to the entirety of the flow path
 322 to avoid sampling of PFBS by other instruments. Additionally, there is evidence that PFBS degrades at temperatures above
 323 400°C (Xiao et al., 2020), and so its ultimately efficacy and reproducibility within the furnace system would be uncertain).
 324 Further, the high operating temperature of the furnace would also be expected to minimize HCl-wall interactions within the
 325 quartz tubing. Indeed, no line losses were found at 11% relative humidity between when the HCl permeation source standard
 326 was injected into the sampling line before the heated furnace (2.95 ± 0.02 ppbv) and when HCl was injected just before the
 327 inertial inlet (accounting for dilution factors) (2.95 ± 0.02 ppbv), consistent with Halfacre et al. (2023). Similar results were
 328 found at 44% relative humidity (pre-furnace value of 2.68 ± 0.03 ppbv vs 2.66 ± 0.03 ppbv when HCl was introduced at inlet),
 329 and real HCl loss was quantified at 66% relative humidity (pre-furnace value of 1.87 ± 0.03 ppbv vs 1.97 ± 0.03 ppbv when
 330 HCl introduced at inlet). Having accounted for these line losses, ANOVA calculations found no significant differences between
 331 these three slopes as presented in Fig. 3 ($F(2,19) = 0.10, p = 0.902$), indicating consistent performance between TILDAS and
 332 CAPS for detecting ClNO_2 . However, it does not appear to explain the deviation from unity, which will be discussed below.

333 As discussed in Sect. 2.1, chemistry may occur within the slurry to produce N_2O_4 , which can easily degrade at room
 334 temperature to produce two NO_2 molecules. If the N_2O_4 output from the $\text{NO}_2^-/\text{Cl}^-$ slurry is constant over the timescale of an
 335 experiment (< 1 hr), it would be expected this additional NO_2 is readily accounted for during blank subtraction calculations.
 336 While we believe this is largely true for the experiments presented above, discrepancies in ClNO_2 signals were observed as
 337 the slurry aged (>~3 weeks), with CAPS-observed NO_2 mixing ratios growing in significant excess of TILDAS-observed HCl
 338 mixing ratios (Fig. A32). Separate applications of TILDAS- and CAPS-based calibration factors (using data from Fig. 5) to

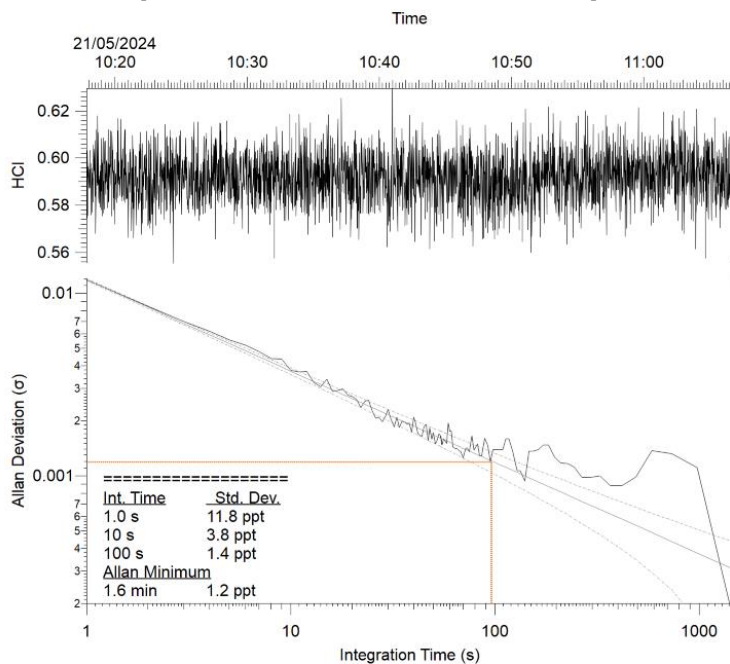
339 concurrent CIMS ClNO_2 observations show closer resemblance to the TILDAS-observed mixing ratios (Fig. A23), suggesting
 340 additional chemistry may be occurring within the salt bed that produces stable reservoirs of NO_2 that thermally dissociate in
 341 the furnace to produce undesired NO_2 . This NO_2 artefact serves as a likely explanation for the sub-unity slopes presented in
 342 Fig. 5, as it would positively bias the CAPS measurements but not the TILDAS, which is only sensitive to HCl. [Thaler et al.](#)
 343 [\(2011\) present in great detail strategies for minimizing \$\text{N}_2\text{O}_4\$ production in their study by minimizing the residence time in](#)
 344 [their \$\text{ClNO}_2\$ generator \(0.3 s herein\) and adjusting the molar ratio of \$\text{Cl}:\text{NO}_2^-\$ of their salt bed \(100:1 herein\), but were](#)
 345 [ultimately unable to completely eliminate it; while we found these strategies helpful for reducing the overall \$\text{NO}_2\$ background](#)
 346 [as measured by CAPS, we found they were unsuccessful in eliminating the artefact when sample gas was passed through the](#)
 347 [heated furnace.](#)

348 We are not aware of such chemistry being addressed in the literature for this ClNO_2 generation method and do not propose potential reactions as it is outside the scope of this paper.

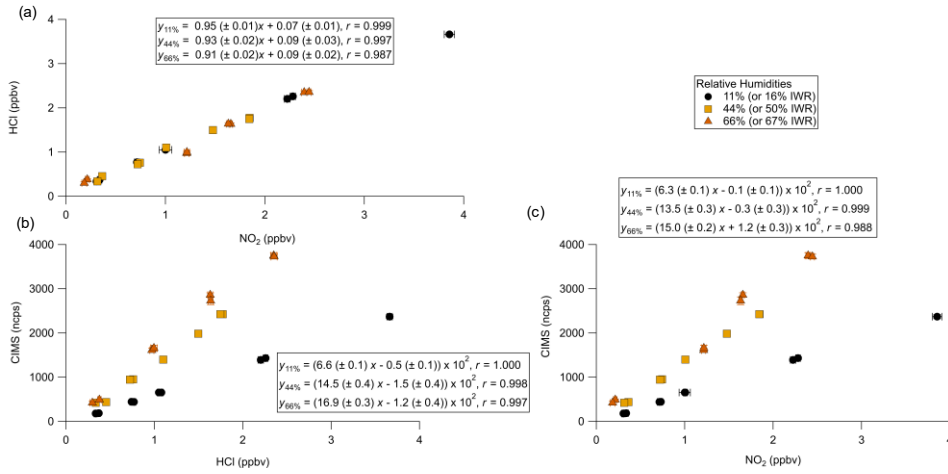


349
 350 Figure 3: a) Time series demonstrating the reversible thermal conversion of ClNO_2 to NO_2 (red trace, CAPS) and HCl (blue trace, TILDAS), as evidenced by changes in CIMS-observed ICINO_2^- (black). Gaps in CIMS data are from internal CIMS tests not
 351 pertinent to this work.
 352
 353 Both HCl and NO_2 mixing ratios independently correlated strongly with the CIMS measurement of ICINO_2^- (Fig. 5b, c), and the I- CIMS sensitivity for ICINO_2^- was found to vary strongly with humidity, as previously reported (Kercher et al., 2009; Mielke et al., 2011). The weakest Pearson correlation coefficient was for NO_2 and ICINO_2^- at 66% relative humidity (r

356 = 0.988), virtually matching that of NO_2 and HCl at the same humidity. Due to the uncertainty / unreliability of the NO_2 as it
 357 relates to ClNO_2 quantitation, we do not further consider the relationship between CAPS and CIMS.



358 **Figure 4:** Allan-Werle plot for TD-TILDAS during addition of ClNO_2 standard into the sample line.
 The Allan minimum is indicated by the dotted red lines.



360

Figure 5 – Comparison curves of a) TILDAS vs CAPS, b) CIMS vs TILDAS, and c) CIMS vs CAPS for injections of varied mixing ratios of ClNO_2 across different relative humidities. Regressions involving TILDAS data have been corrected for line losses observed at 66% relative humidity.

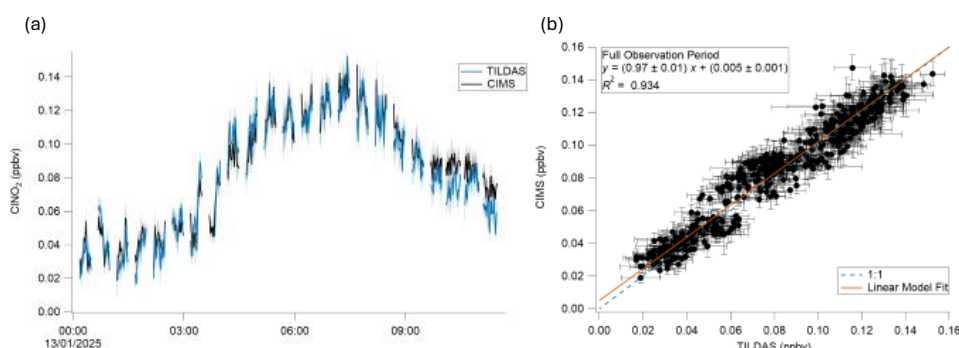
The linear equations from Fig. 5a present significant intercepts that suggest a source of positive error for the TILDAS, and the similarity of these intercepts suggest a relatively constant/consistent source (values are statistically the same $F(4,19) = 0.624$, $p = 0.546$ per ANOVA). For these experiments, TILDAS blanks were obtained by sampling slurry air flowed through an unheated furnace; in this scenario, Reactions R1-R2 are unable to occur, and therefore any signal observed by TILDAS could be considered background. It is possible that a small amount of HCl forms in the slurry system from the aqueous disproportion reaction between Cl_2 and H_2O . When the furnace is unheated, some amount of HCl interaction with the quartz tubing is expected given there is no PFBS flow through this portion of the plumbing, biasing this blank measurement low. Then, once the furnace is heated to 450 °C, this HCl will be liberated from the quartz tubing, possibly then biasing the heated measurement high. This is supported by the presence of a peak in observed HCl as the furnace reheats (e.g., as in the second temperature ramp in Fig. 3), as some of the HCl sorbed to the furnace tube walls under room temperature is forced into the gas phase. The statistical similarity in intercepts implies this effect is constant across these experiments, leading to a consistent offset. While an ideal blank would sample the gas downstream of the slurry while selectively scrubbing ClNO_2 , this was not practical to achieve without simultaneously scrubbing HCl. Therefore, we propose the y-intercept in these cases is a good estimate of the systematic error present in these comparison experiments.

3.3 Applicability as Field Instrument

The applicability of TD-TILDAS as a field method for ClNO_2 detection was tested by sampling ambient air from outside the Wolfson Atmospheric Chemistry Laboratory building on the University of York campus (York, United Kingdom) from the morning of 13 January 2025 (Fig. 6). Compared with the laboratory-based configuration described in Sect. 3.2, ambient air will contain varied amounts of HCl that would interfere with accurate quantification of ClNO_2 via the TILDAS method. To address this, a base-coated denuder (Sect. 2.2) was installed in the HCl sampling line. ClNO_2 throughput was found to be

384 hindered when flowed through the denuder but increased over the course of the observation period (pre-experiment estimation
 385 of 55% loss on 10 January vs 31% measured directly after the experiment on 13 January). This loss was accounted for by
 386 applying a time-varying, linearly interpolated correction factor for the denuder. In addition, line losses affecting HCl between
 387 the heated furnace and TILDAS inlet were estimated as 2.7%, which was added back into the TILDAS measurements. CIMS
 388 observations of ClNO_2^- were calibrated against TD-TILDAS using a mid-experiment ClNO_2 addition, yielding a sensitivity
 389 factor of 1982 ncps ppb $^{-1}$ (measured with a corresponding IWR of 42%). We note that this factor is ~35% greater than the
 390 value of 1450 ncps ppb $^{-1}$ as presented in Fig. 5b for a comparable IWR (44%); this is likely due to the replacement of the
 391 reagent ion permeation source, repair of reagent ion source heaters, and change in the overall sampling CIMS inlet
 392 configuration between the experiments from Sect. 3.2 and this section (as illustrated by Fig. 1). Application of this sensitivity
 393 factor across this measurement period can be justified as the IWR was found to be stable ($38 \pm 2\%$). Limits of detection, based
 394 on instrument blanks, were found to average 10 ± 5 pptv for TD-TILDAS and 1 ± 1 pptv for CIMS (using 60 second data
 395 averaging).

396 As seen in Fig. 6a, TILDAS- and CIMS-observed ClNO_2 demonstrate very good agreement for these ambient
 397 observations in both signal magnitude and structure. This is quantitatively supported by regression calculations during this
 398 period that yield a slope of 0.97 ± 0.01 (Fig. 6b), which is well within the averaged combined uncertainty for this period of
 399 9%. While the sub-unity slope could indicate small losses on the TILDAS method, pre- and post-experimental losses were
 400 tested and corrected for as detailed above, and so this is not believed to be a large source of error in this case. It is otherwise
 401 not unexpected that this slope is found to deviate from unity given the uncertainty in the application of a single-point CIMS
 402 sensitivity factor. Nevertheless, this agreement gives us confidence that it is appropriate for these measurements and provides
 403 proof-of-concept for this TILDAS method.



405
 406 **Figure 6 – a)** Time series comparison of TILDAS and CIMS observations of ClNO_2 . **b)** Scatter plot of data shown in panel (a). The
 407 error shading in (a) and bars in (b) represent the standard deviation of the 60 s averaged measurements.

408 Additional sources of measurement uncertainty include unaccounted-for thermolabile chlorine reservoirs that could
 409 cause positive interference in the TILDAS-method. As stated above, the TD-TILDAS method functions on the assumption
 410 that ClNO_2 is the only major inorganic chlorine source that thermally dissociates at 450 °C. As shown by the model, ClNO_2
 411 may be a potential source of interference if present (Fig. A2), while However, relevant thermochemistry information is was
 412 unavailable for organochlorides and chloramines, which therefore cannot be ruled out as possible interferences by modeling.
 413 Indeed, while CIMS signals of ClNO and chloramines did not rise above their baselines during the period shown in Fig. 6, a

414 separate measurement period demonstrates multiple occurrences where signal increases in iodide-tri- and di-chloramine
 415 adducts (INCl_3^- , INHCl_2^-) correspond with TILDAS-observed signal increases (Fig. A43). This is most dramatic at ~08:15,
 416 where ~115 ncp of INCl_3^- and 18 ncp of INHCl_2^- corresponds with an increase of 100 pptv in the TILDAS signal. While
 417 these chloramine observations cannot be quantified at this time, trichloramine and dichloramine has previously been detected
 418 in downtown Toronto at ≤ 0.104 ppb and ≤ 8 ppbv, respectively (Wang et al., 2023), suggesting a combined 100 pptv
 419 interference contribution from these compounds is realistic. Synthesis and calibration of chloramine standards is a non-trivial
 420 task (Wang et al., 2023), and so further experiments are required to investigate 1) to what extent the chloramine signals can be
 421 quantified by TILDAS and 2) if the chloramine signal can be dissected from the ClNO_2 signal through temperature scans. The
 422 results of such experiments may therefore allow this method to be extended for the quantification of both chloramines and
 423 ClNO_2 .

424 While organochlorides (e.g., CH_3Cl , CH_2Cl_2 , CHCl_3 , and CCl_4) were not explicitly measured during the period in
 425 Fig. 6, it would be expected that their potential interference in the TILDAS signal (if they dissociate in the furnace) would
 426 present as a slow varying background signal that appears as an offset above a blank, given the ubiquity of these compounds
 427 and relatively long tropospheric lifetimes for CH_3Cl , CH_2Cl_2 , CHCl_3 , and CCl_4 of 1 year, 6 months, 6 months, and 124 years,
 428 respectively (World Meteorological Organization, 2022). Such an offset, if present, could be quantified during daytime
 429 measurements (i.e., when no ClNO_2 will be present in the boundary layer) and readily subtracted from nighttime measurements
 430 if necessary. However, the agreement between TILDAS and CIMS measurements as presented in Fig. 6 suggests this
 431 interference is not present, providing some evidence that these organochlorides are not dissociating in the furnace.

432 Conclusions

433 This work demonstrates the viability of TD-TILDAS as an independent ClNO_2 detection method at performance metrics
 434 comparable to quadrupole CIMS, which are more than adequate for commonly observed mixing ratios in the boundary layer.
 435 While modern CIMS instruments can achieve lower limits of detection and higher precision, the major advantage of TD-
 436 TILDAS over CIMS is that it does not require external ClNO_2 calibration experiments, as this work demonstrates the unity
 437 conversion of ClNO_2 to HCl that is subsequently detected based on well-understood spectroscopic principles. The TD method
 438 described here can thus be used effectively in laboratory settings to measure ClNO_2 in related experiments, or even to calibrate
 439 CIMS for ClNO_2 directly without needing to make assumptions regarding Cl_2 conversion on salt slurries. Additionally, use of
 440 a denuder allows this method to be readily applied to other HCl optical instruments, such as those based on CRDS.

441 As a field method, TD-TILDAS demonstrated excellent agreement with a co-located CIMS for ClNO_2 detection. The
 442 method is reliant on accurate and regular characterization of ClNO_2 throughput through the denuder, which was found to
 443 increase across four days of sampling. Longer-term measurement campaigns would benefit from at least weekly denuder
 444 replacements to ensure acidic gases are consistently scrubbed and do not interfere with ClNO_2 observations. However, the TD-
 445 TILDAS method appears susceptible to positive interference, potentially resulting from chloramines, or other unaccounted-
 446 for thermolysable chlorine compounds. Care should thus be taken should this method be deployed where large amounts of
 447 chloramines are known to be present, such as swimming pools or near water treatment facilities. More work is still required
 448 to confirm and quantify the response of this method to chloramine and organochlorides, and if so, identify an appropriate
 449 method to mitigate this potential interference. While modelling additionally suggests ClNO as an interferent, its presence in
 450 the boundary layer is yet to be confirmed through in situ observations. In any case, careful temperature ramps (e.g., Day et al.,
 451 2002) performed with the furnace in environments where unknown interferences may be a concern would likely reveal the
 452 purity of the ClNO_2 signal observed. Experimental adjustments could be further made for the TILDAS to alternate its sampling

453 between a heated channel (as described in this paper) for ClNO_2 detection and an unheated pathway that allows for the
454 additional detection of HCl. Doing so would require careful characterization of physical HCl losses inherent to both sampling
455 pathways, as well as consideration of the likely hysteresis in detected HCl mixing ratios resulting from changes to the sampled
456 air temperature that would affect the partitioning of HCl between surfaces and the gas phase.

457

458

459 Appendix A

460 Table A1 – Bimolecular reactions and parameters used for the modelling described in Sect. 2.5. Reactions follow the rate expression
461 $k(T) = A (T/298)^n e^{-E_a/RT}$ (Burkholder et al., 2015)

Reaction	A	n	Ea (kJ mol ⁻¹)	Reference
ClNO ₂ + M ==> Cl + NO ₂	9.13 x 10 ⁻¹⁰	0	106	(Baulch et al., 1981)
Cl + Cl ==> Cl ₂	6.15 x 10 ⁻³⁴	0	-7.53	(Baulch et al., 1981)
M + ClONO ₂ ==> NO ₂ + ClO	2.76 x 10 ⁻⁵	0	94.78	(Anderson and Fahey, 1990)
CH ₄ + Cl ==> CH ₃ + HCl	8.24 x 10 ⁻¹³	2.49	5.06	(Bryukov et al., 2002)
HCl + OH ==> H ₂ O + Cl	3.74 x 10 ⁻¹²	0	4.27	(Baulch et al., 1981)
HCl + M ==> H + Cl	7.31 x 10 ⁻¹¹	0	342	(Baulch et al., 1981)
CH ₃ + HCl ==> CH ₄ + Cl	3.89 x 10 ⁻¹³	0	9.64	(Baulch et al., 1981)
CH ₃ + NO ₂ ==> CH ₃ O + NO	3.44 x 10 ⁻¹¹	0	0	(Srinivasan et al., 2005)
O ₃ + M ==> O + O ₂	7.6 x 10 ⁻¹⁰	0	93.12	(Heimerl and Coffee, 1979)
CH ₃ + O ==> CH ₂ O + H	2.26 x 10 ⁻¹¹	0	0	(Baulch et al., 1992)
HCl + O ==> OH + Cl	7.07 x 10 ⁻¹⁴	2.87	14.72	(Mahmud et al., 1990)
OH + CH ₄ ==> CH ₃ + H ₂ O	4.16 x 10 ⁻¹³	2.18	10.24	(Srinivasan et al., 2005)
Cl ₂ + M ==> Cl + Cl	3.85 x 10 ⁻¹¹	0	196	(Baulch et al., 1981)
Cl + Cl ==> Cl ₂	6.15 x 10 ⁻³⁴	0	-7.53	(Baulch et al., 1981)
Cl ₂ + O ==> ClO + Cl	4.17 x 10 ⁻¹²	0	11.39	(Baulch et al., 1981)
Cl ₂ + H ==> HCl + Cl	1.43 x 10 ⁻¹⁰	0	4.91	(Baulch et al., 1981)
Cl ₂ + OH ==> HOCl + Cl	3.60 x 10 ⁻¹²	0	9.98	(Atkinson et al., 2007)
CH ₃ + O ₂ ==> CH ₃ O + O	2.19 x 10 ⁻¹⁰	0	131	(Baulch et al., 1992)
ClO + O ==> O ₂ + Cl	2.50 x 10 ⁻¹¹	0	-0.91	(Atkinson et al., 2007)
OH + ClO ==> HO ₂ + Cl	6.86 x 10 ⁻¹²	0	-2.49	(Atkinson et al., 2007)
OH + ClO ==> HCl + O ₂	4.38 x 10 ⁻¹³	0	-2.49	(Atkinson et al., 2007)

$\text{CH}_3\text{O} + \text{NO} \rightleftharpoons \text{CH}_2\text{O} + \text{HNO}$	4.00×10^{-12}	-0.7	0	(Atkinson et al., 1992)
$\text{CH}_3\text{O} + \text{O}_2 \rightleftharpoons \text{CH}_2\text{O} + \text{HO}_2$	7.20×10^{-14}	0	8.98	(Atkinson et al., 1992)
$\text{HOCl} + \text{O} \rightleftharpoons \text{OH} + \text{ClO}$	1.70×10^{-13}	0	0	(Atkinson et al., 2007)
$\text{CICO} + \text{M} \rightleftharpoons \text{CO} + \text{Cl}$	4.10×10^{-10}	0	24.6	(Atkinson et al., 2007)
$\text{O}_3 + \text{NO} \rightleftharpoons \text{O}_2 + \text{NO}_2$	1.40×10^{-12}	0	10.9	(Atkinson et al., 2004)
$\text{CH}_3\text{O}_2 + \text{NO} \rightleftharpoons \text{CH}_3\text{O} + \text{NO}_2$	2.30×10^{-12}	0	-2.99	(Atkinson et al., 2006b)
$\text{HO}_2 + \text{NO} \rightleftharpoons \text{NO}_2 + \text{OH}$	3.6×10^{-12}	0	-2.24	(Atkinson et al., 2004)
$\text{CH}_2\text{O} + \text{Cl} \rightleftharpoons \text{HCl} + \text{HCO}$	8.20×10^{-11}	0	0.28	(Atkinson et al., 1992)
$\text{CH}_2\text{O} + \text{OH} \rightleftharpoons \text{HCO} + \text{H}_2\text{O}$	4.73×10^{-12}	1.18	-1.87	(Baulch et al., 1992)
$\text{CH}_3\text{O}_2 + \text{HO}_2 \rightleftharpoons \text{CH}_3\text{OOH} + \text{O}_2$	3.80×10^{-13}	0	-6.49	(Atkinson et al., 1992)
$\text{CH}_3\text{OOH} \rightleftharpoons \text{CH}_3\text{O} + \text{OH}$	6.00×10^{14}	0	177	(Baulch et al., 1994)
$\text{HCO} + \text{O}_2 \rightleftharpoons \text{CO} + \text{HO}_2$	5.20×10^{-12}	0	0	(Atkinson et al., 2006b)
$\text{CO} + \text{OH} \rightleftharpoons \text{CO}_2 + \text{H}$	5.40×10^{-14}	1.5	-2.08	(Baulch et al., 1992)
$\text{Cl} + \text{HO}_2 \rightleftharpoons \text{HCl} + \text{O}_2$	1.80×10^{-11}	0	-1.41	(Atkinson et al., 1992)
$\text{Cl} + \text{HO}_2 \rightleftharpoons \text{ClO} + \text{OH}$	6.30×10^{-11}	0	4.74	(Atkinson et al., 2007)
$\text{Cl} + \text{O}_3 \rightleftharpoons \text{ClO} + \text{O}_2$	2.80×10^{-11}	0	2.08	(Atkinson et al., 2007)
$\text{CO} + \text{Cl} \rightleftharpoons \text{CICO}$	1.33×10^{-33}	-3.8	0.00	(Atkinson et al., 2007)
$\text{OH} + \text{HOCl} \rightleftharpoons \text{H}_2\text{O} + \text{ClO}$	5.00×10^{-13}	0	0	(Atkinson et al., 2007)
$\text{ClO} + \text{HO}_2 \rightleftharpoons \text{HOCl} + \text{O}_2$	2.20×10^{-12}	0	-2.8	(Atkinson et al., 2007)
$\text{ClO} + \text{ClO} \rightleftharpoons \text{Cl}_2 + \text{O}_2$	1.00×10^{-12}	0	13.22	(Atkinson et al., 2007)
$\text{ClO} + \text{ClO} \rightleftharpoons \text{OCIO} + \text{Cl}$	3.50×10^{-13}	0	11.39	(Atkinson et al., 2007)
$\text{ClO} + \text{ClO} \rightleftharpoons \text{ClOO} + \text{Cl}$	3.00×10^{-11}	0	20.37	(Atkinson et al., 2007)
$\text{ClO} + \text{NO} \rightleftharpoons \text{Cl} + \text{NO}_2$	6.20×10^{-12}	0	-2.45	(Atkinson et al., 2007)
$\text{CH}_2\text{O} + \text{O} \rightleftharpoons \text{HCO} + \text{OH}$	1.78×10^{-11}	0.57	11.56	(Baulch et al., 1992)

OH + NO ₂ ==> HNO ₃	2.70 x 10 ⁻¹¹	0	0	(Troe, 2012)
CH ₃ Cl + OH ==> CH ₂ Cl + H ₂ O	1.40E-12	1.6	8.65	(Cohen and Westberg, 1991)
CH ₃ Cl + H ==> CH ₃ + HCl	6.14E-11	0	38.9	(Westenberg and deHaas, 1975)
CH ₃ Cl + CH ₃ ==> CH ₄ + CH ₂ Cl	2.09E-12	0	48.6	(Macken and Sidebottom, 1979)
CH ₃ Cl + Cl ==> CH ₂ Cl + HCl	3.30E-11	0	10.39	(Atkinson et al., 2008)
CHCl ₃ + Cl ==> CCl ₃ + HCl	4.90E-12	0	10.31	(Atkinson et al., 2008)
Cl + C ₃ H ₆ ==> Products	2.70E-10	0	0	(Atkinson et al., 2006b)
Cl + C ₅ H ₈ ==> Products	4.30E-10	0	0	(Orlando et al., 2003)
CINO + M ==> Cl + NO	2.16E-09	0	134	(Baulch et al., 1981)

464 Table A2 – Termolecular reactions and parameters used for the modelling described in Sect. 2.5. The effective rate constant is
 465 calculated by combining the low- and high-pressure limit expressions into the following formula: $k_f(T, [M]) =$
 466 $\left\{ \frac{k_\infty(T)k_0(T)[M]}{k_\infty(T)+k_0(T)[M]} \right\} 0.6^{\left(1+\left[\log_{10}\left(\frac{k_0(T)[M]}{k_\infty(T)}\right)\right]^2\right)^{-1}}$

Reaction	Low-Pressure Limit $k_0 = k_0^{298}(T/298)^{-n}$		High Pressure Limit $k_\infty = k_\infty^{298}(T/298)^{-n}$		Reference
	k_0^{298}	n	k_∞^{298}	m	
$\text{Cl} + \text{NO}_2 + \text{M} \implies \text{ClNO}_2 + \text{M}$	1.8×10^{-31}	2	1.1×10^{-10}	1	(Burkholder et al., 2015)
$\text{CH}_3 + \text{O}_2 + \text{M} \implies \text{CH}_3\text{O}_2 + \text{M}$	4.1×10^{-31}	3.6	1.2×10^{-12}	-1.1	(Burkholder et al., 2015)
<u>$\text{Cl} + \text{C}_2\text{H}_4 + \text{M} \implies \text{Products}$</u>	<u>1.6×10^{-29}</u>	<u>3.3</u>	<u>3.1×10^{-10}</u>	<u>1</u>	(Burkholder et al., 2015)

467

468

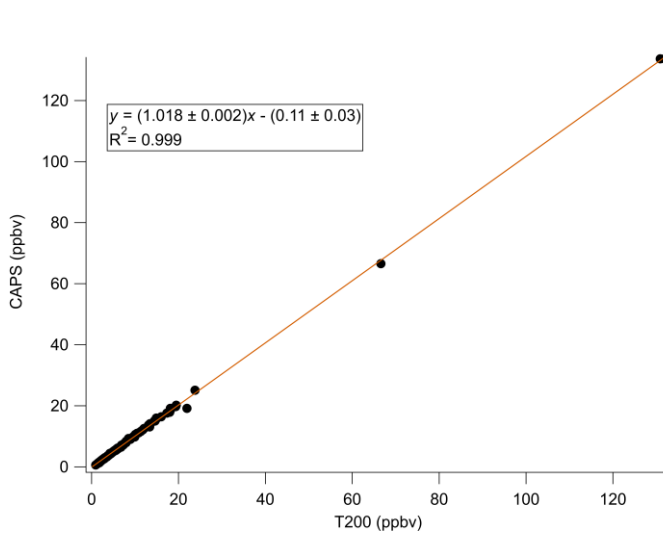
469

470 **Table A3 – Initial concentrations for specified species simulated in model, and listed mixing ratios are based on a temperature of 20**
 471 **°C. Potential interferents were tested in separate model runs according to the groupings on each line below, and were otherwise**
 472 **initiated with a concentration of 0 molecules cm⁻³. All other compounds were initialised with a concentration of 0 molecules cm⁻³.**

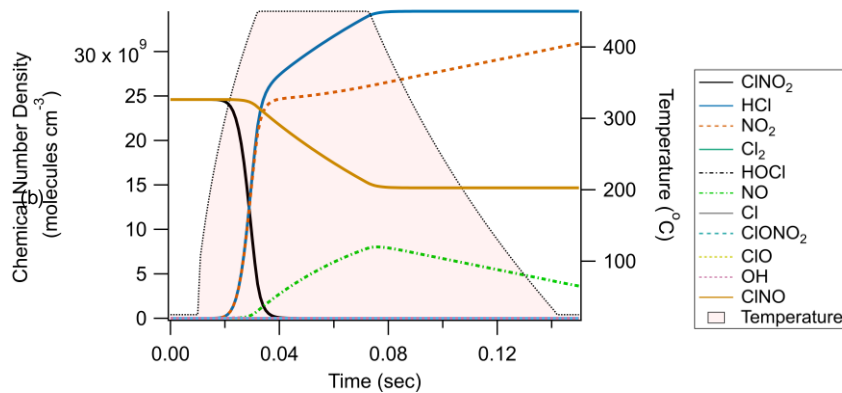
Species	Initial Concentration (molecules cm ⁻³)
CINO ₂	2.46×10^{10} (1 ppbv)
N ₂	1.92×10^{19} (78%)
O ₂	5.17×10^{19} (21%)
CH ₄	4.92×10^{13} (2000 ppmwppbv)
OH	1×10^6
O ₃	9.84×10^{11} (40 ppbv)
Potential Interferents	
CINO	<u>2.46×10^{10} (1 ppbv)</u>
Ethene, Propene, Isoprene	<u>1.23×10^{12} (50 ppbv)</u>

473

474



(a)

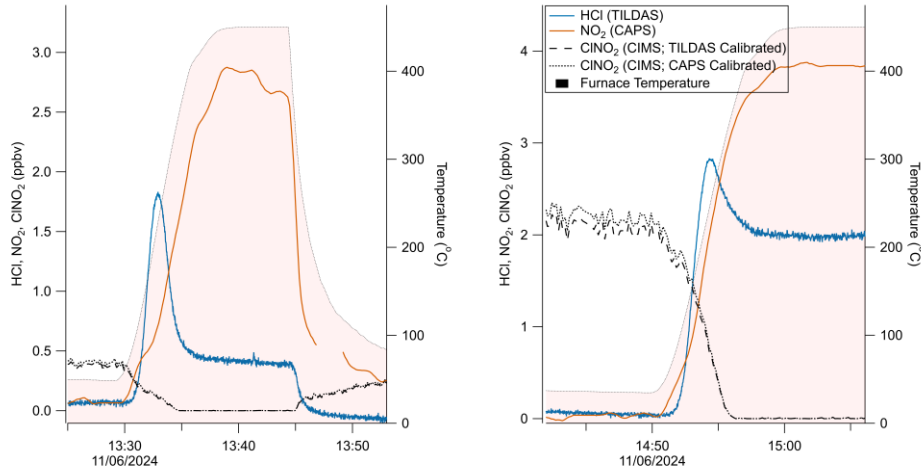


480

481

482

483

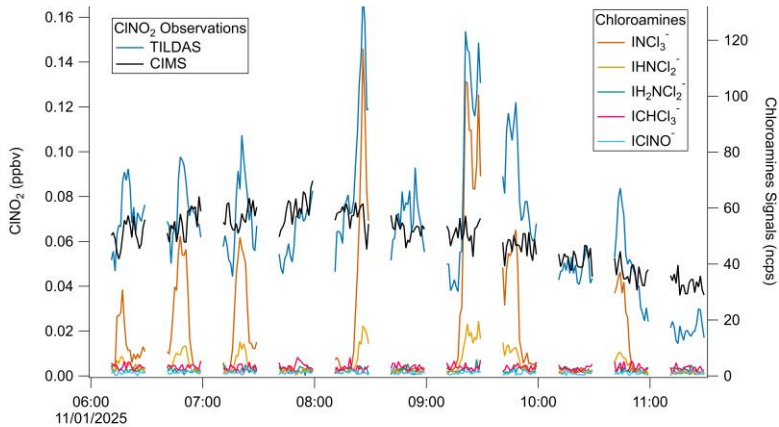


484

485 **Figure A23** – a) Comparison plot of CINO₂ observations with an apparent excess of NO₂ formed after aging/processing of the same
 486 slurry used for generating Fig. 3-4. (b) Additional comparison using a freshly made slurry. CIMS signal was calibrated using
 487 humidity-dependent calibration factors as presented in Fig. 5.

488

489



490
 491 **Figure A34** –Field data showing apparent coincident signal increases TILDAS-observed CINO_2 with CIMS-observed chloramines,
 492 ICINO^- , and ICHCl_3^- (uncalibrated).

493 Formatted: Superscript

Formatted: Subscript

Formatted: Superscript

494 **Code availability**

495 Code used for this analysis is available from the corresponding author on request.

496 **Data availability**

497 Data are available from the corresponding author on request.

498 **Author contribution**499 PRV, MAR, SSB designed and performed proof-of-concept experiments to demonstrate potential of the method.
500 SCH, HRR, CD, TIY designed, built, and tested the HCl TILDAS at Aerodyne Research, Inc. SCH, HRR, CD, TIY, and PME
501 designed initial laboratory experiments.
502 JWH and PME designed laboratory and field experiments, and JWH conducted laboratory and field experiments presented in
503 this work.
504 LM, MDS, LJC provided support for laboratory use of CIMS. EM, TJB, HC provided support for field CIMS observations.
505 JWH prepared the manuscript, and all authors reviewed the manuscript.
506507 **Competing interests**

508 The authors declare that they have no conflicts of interest.

509 **Acknowledgements**510 The authors would also like to thank Abigail Mortimer for her glassblowing services, Stephen Andrews and Stuart Young for
511 assistance with creating custom furnaces. Additionally, the authors thank William Drysdale and Katie Read for assistance with
512 calibrating and using the York CAPS instrument. Further, the authors thank Michael Agnese and Michael Moore for TILDAS
513 technical support.
514515 **Financial Support**

516 This research has been supported by the European Research Council (H2020, grant no. ERC-StG 802685).

517 **References**518 A. Angelucci, A., R. Crilley, L., Richardson, R., E. Valkenburg, T. S., S. Monks, P., M. Roberts, J., Sommariva, R., and
519 C. VandenBoer, T.: Elevated levels of chloramines and chlorine detected near an indoor sports complex, Environmental
520 Science: Processes & Impacts, 25, 304–313, <https://doi.org/10.1039/D2EM00411A>, 2023.
521 Anderson, L. and Fahey, D.: Studies with nitryl hypochlorite: Thermal dissociation rate and catalytic conversion to nitric oxide
522 using an NO/O₃ chemiluminescence detector, Journal of Physical Chemistry, 94, 644–652, 1990.

523 Atkinson, R., Baulch, D. L., Cox, R. A., Hampson, R. F., Jr., Kerr, J. A., and Troe, J.: Evaluated Kinetic and Photochemical
 524 Data for Atmospheric Chemistry: Supplement IV, IUPAC Subcommittee on Gas Kinetic Data Evaluation for Atmospheric
 525 Chemistry, *Journal of Physical and Chemical Reference Data*, 21, 1125, <https://doi.org/10.1063/1.555918>, 1992.

526 Atkinson, R., Baulch, D. L., Cox, R. A., Crowley, J. N., Hampson, R. F., Hynes, R. G., Jenkin, M. E., Rossi, M. J., and Troe,
 527 J.: Evaluated kinetic and photochemical data for atmospheric chemistry: Volume I - gas phase reactions of O_x, HO_x, NO_x and
 528 SO_x species, *Atmospheric Chemistry and Physics*, 4, 1461–1738, <https://doi.org/10.5194/acp-4-1461-2004>, 2004.

529 Atkinson, R., Baulch, D. L., Cox, R. A., Crowley, J. N., Hampson, R. F., Hynes, R. G., Jenkin, M. E., Rossi, M. J., Troe, J.,
 530 and IUPAC Subcommittee: Evaluated kinetic and photochemical data for atmospheric chemistry: Volume II - gas phase
 531 reactions of organic species, *Atmospheric Chemistry and Physics*, 6, 3625–4055, <https://doi.org/10.5194/acp-6-3625-2006>,
 532 2006a.

533 Atkinson, R., Baulch, D. L., Cox, R. A., Crowley, J. N., Hampson, R. F., Hynes, R. G., Jenkin, M. E., Rossi, M. J., Troe, J.,
 534 and IUPAC Subcommittee: Evaluated kinetic and photochemical data for atmospheric chemistry: Volume II - gas phase
 535 reactions of organic species, *Atmospheric Chemistry and Physics*, 6, 3625–4055, <https://doi.org/10.5194/acp-6-3625-2006>,
 536 2006b.

537 Atkinson, R., Baulch, D. L., Cox, R. A., Crowley, J. N., Hampson, R. F., Hynes, R. G., Jenkin, M. E., Rossi, M. J., and Troe,
 538 J.: Evaluated kinetic and photochemical data for atmospheric chemistry: Volume III - gas phase reactions of inorganic
 539 halogens, *Atmospheric Chemistry and Physics*, 7, 981–1191, <https://doi.org/10.5194/acp-7-981-2007>, 2007.

540 Atkinson, R., Baulch, D. L., Cox, R. A., Crowley, J. N., Hampson, R. F., Hynes, R. G., Jenkin, M. E., Rossi, M. J., Troe, J.,
 541 and Wallington, T. J.: Evaluated kinetic and photochemical data for atmospheric chemistry: Volume IV – gas phase reactions
 542 of organic halogen species, *Atmospheric Chemistry and Physics*, 8, 4141–4496, <https://doi.org/10.5194/acp-8-4141-2008>,
 543 2008.

544 Bannan, T. J., Booth, A. M., Bacak, A., Muller, J. B. A., Leather, K. E., Le Breton, M., Jones, B., Young, D., Coe, H., Allan,
 545 J., Visser, S., Slowik, J. G., Furger, M., Prévôt, A. S. H., Lee, J., Dunmore, R. E., Hopkins, J. R., Hamilton, J. F., Lewis, A.
 546 C., Whalley, L. K., Sharp, T., Stone, D., Heard, D. E., Fleming, Z. L., Leigh, R., Shallcross, D. E., and Percival, C. J.: The
 547 first UK measurements of nitrily chloride using a chemical ionization mass spectrometer in central London in the summer of
 548 2012, and an investigation of the role of Cl atom oxidation, *Journal of Geophysical Research: Atmospheres*, 120, 5638–5657,
 549 <https://doi.org/10.1002/2014JD022629>, 2015.

550 Baulch, D. L., Duxbury, J., Grant, S., and Montague, D. C.: Evaluated kinetic data for high temperature reactions. Volume 4.
 551 Homogeneous gas phase reactions of halogen- and cyanide- containing species, *J. Phys. Chem. Ref. Data*, 10, 1–721, 1981.

552 Baulch, D. L., Cobos, C. J., Cox, R. A., Esser, C., Frank, P., Just, Th., Kerr, J. A., Pilling, M. J., Troe, J., Walker, R. W., and
 553 Warnatz, J.: Evaluated Kinetic Data for Combustion Modelling, *Journal of Physical and Chemical Reference Data*, 21, 411,
 554 <https://doi.org/10.1063/1.555908>, 1992.

555 Baulch, D. L., Cobos, C. J., Cox, R. A., Frank, P., Hayman, G., Just, Th., Kerr, J. A., Murrells, T., Pilling, M. J., Troe, J.,
 556 Walker, R. W., and Warnatz, J.: Evaluated Kinetic Data for Combustion Modeling. Supplement I, *Journal of Physical and
 557 Chemical Reference Data*, 23, 847–848, <https://doi.org/10.1063/1.555953>, 1994.

558 Bryukov, M. G., Slagle, I. R., and Knyazev, V. D.: Kinetics of Reactions of Cl Atoms with Methane and Chlorinated Methanes,
 559 *J. Phys. Chem. A*, 106, 10532–10542, <https://doi.org/10.1021/jp0257909>, 2002.

560 Budisulistiorini, S. H., Li, X., Bairai, S. T., Renfro, J., Liu, Y., Liu, Y. J., McKinney, K. A., Martin, S. T., McNeill, V. F., Pye,
 561 H. O. T., Nenes, A., Neff, M. E., Stone, E. A., Mueller, S., Knote, C., Shaw, S. L., Zhang, Z., Gold, A., and Surratt, J. D.:
 562 Examining the effects of anthropogenic emissions on isoprene-derived secondary organic aerosol formation during the 2013
 563 Southern Oxidant and Aerosol Study (SOAS) at the Look Rock, Tennessee ground site, *Atmospheric Chemistry and Physics*,
 564 15, 8871–8888, <https://doi.org/10.5194/acp-15-8871-2015>, 2015.

565 Burkholder, J. B., Sander, S. P., Abbott, J., Barker, J. R., Huie, R. E., Kolb, C. E., Kurylo, M. J., Orkin, V. L., Wilmouth, D.
 566 M., and Wine, P. H.: Chemical Kinetics and Photochemical Data for Use in Atmospheric Studies, Evaluation No. 18, JPL
 567 Publication 15-10., Jet Propulsion Laboratory, Pasadena, 2015.

568 Cantrell, C. A.: Technical Note: Review of methods for linear least-squares fitting of data and application to atmospheric
 569 chemistry problems, *Atmospheric Chemistry and Physics*, 8, 5477–5487, <https://doi.org/10.5194/acp-8-5477-2008>, 2008.

570 Cohen, N. and Westberg, K. R.: Chemical Kinetic Data Sheets for High-Temperature Reactions. Part II, Journal of Physical
571 and Chemical Reference Data, 20, 1211–1311, <https://doi.org/10.1063/1.555901>, 1991.

572 Darwent, B. B.: Bond Dissociation Energies in Simple Molecules, U.S. National Bureau of Standards, 1970.

573 Day, D. A., Wooldridge, P. J., Dillon, M. B., Thornton, J. A., and Cohen, R. C.: A thermal dissociation laser-induced
574 fluorescence instrument for in situ detection of NO₂, peroxy nitrates, alkyl nitrates, and HNO₃, Journal of Geophysical
575 Research: Atmospheres, 107, ACH 4-1-ACH 4-14, <https://doi.org/10.1029/2001JD000779>, 2002.

576 Decker, Z. C. J., Novak, G. A., Aikin, K., Veres, P. R., Neuman, J. A., Bourgeois, I., Bui, T. P., Campuzano-Jost, P., Coggon,
577 M. M., Day, D. A., DiGangi, J. P., Diskin, G. S., Dollner, M., Franchin, A., Fredrickson, C. D., Froyd, K. D., Gkatzelis, G. I.,
578 Guo, H., Hall, S. R., Halliday, H., Hayden, K., Holmes, C. D., Jimenez, J. L., Kupc, A., Lindaas, J., Middlebrook, A. M.,
579 Moore, R. H., Nault, B. A., Nowak, J. B., Pagonis, D., Palm, B. B., Peischl, J., Piel, F. M., Rickly, P. S., Robinson, M. A.,
580 Rollins, A. W., Ryerson, T. B., Schill, G. P., Sekimoto, K., Thompson, C. R., Thornhill, K. L., Thornton, J. A., Ullmann, K.,
581 Warneke, C., Washenfelder, R. A., Weinzierl, B., Wiggins, E. B., Williamson, C. J., Winstead, E. L., Wisthaler, A., Womack,
582 C. C., and Brown, S. S.: Airborne Observations Constrain Heterogeneous Nitrogen and Halogen Chemistry on Tropospheric
583 and Stratospheric Biomass Burning Aerosol, Geophysical Research Letters, 51, e2023GL107273,
584 <https://doi.org/10.1029/2023GL107273>, 2024.

585 Driscoll, C. T., Mason, R. P., Chan, H. M., Jacob, D. J., and Pirrone, N.: Mercury as a Global Pollutant: Sources, Pathways,
586 and Effects, Environ. Sci. Technol., 47, 4967–4983, <https://doi.org/10.1021/es305071v>, 2013.

587 Frenzel, A., Scheer, V., Sikorski, R., George, Ch., Behnke, W., and Zetzsch, C.: Heterogeneous Interconversion Reactions of
588 BrNO₂, CINO₂, Br₂, and Cl₂, J. Phys. Chem. A, 102, 1329–1337, <https://doi.org/10.1021/jp973044b>, 1998.

589 Furlani, T. C., Veres, P. R., Dawe, K. E. R., Neuman, J. A., Brown, S. S., VandenBoer, T. C., and Young, C. J.: Validation of
590 a new cavity ring-down spectrometer for measuring tropospheric gaseous hydrogen chloride, Atmospheric Measurement
591 Techniques, 14, 5859–5871, <https://doi.org/10.5194/amt-14-5859-2021>, 2021.

592 Guelachvili, G., Niay, P., and Bernage, P.: Infrared bands of HCl and DCl by Fourier transform spectroscopy: Dunham
593 coefficients for HCl, DCl, and TCl, Journal of Molecular Spectroscopy, 85, 271–281, [https://doi.org/10.1016/0022-2852\(81\)90200-9](https://doi.org/10.1016/0022-
594 2852(81)90200-9), 1981.

595 Hagen, C. L., Lee, B. C., Franka, I. S., Rath, J. L., VandenBoer, T. C., Roberts, J. M., Brown, S. S., and Yalin, A. P.: Cavity
596 ring-down spectroscopy sensor for detection of hydrogen chloride, Atmospheric Measurement Techniques, 7, 345–357,
597 <https://doi.org/10.5194/amt-7-345-2014>, 2014.

598 Halfacre, J. W. and Simpson, W. R.: Polar Tropospheric Ozone Depletion Events, in: Chemistry in the Cryosphere, vol.
599 Volume 3, WORLD SCIENTIFIC, 411–452, https://doi.org/10.1142/9789811230134_0008, 2022.

600 Halfacre, J. W., Stewart, J., Herndon, S. C., Roscioli, J. R., Dyroff, C., Yacovitch, T. I., Flynn, M., Andrews, S. J., Brown, S.
601 S., Veres, P. R., and Edwards, P. M.: Using tunable infrared laser direct absorption spectroscopy for ambient hydrogen chloride
602 detection: HCl-TILDAS, Atmospheric Measurement Techniques, 16, 1407–1429, <https://doi.org/10.5194/amt-16-1407-2023>,
603 2023.

604 Heimerl, J. M. and Coffee, T. P.: The unimolecular ozone decomposition reaction, Combustion and Flame, 35, 117–123,
605 [https://doi.org/10.1016/0010-2180\(79\)90015-4](https://doi.org/10.1016/0010-2180(79)90015-4), 1979.

606 Hellén, H., Kouznetsov, R., Kraft, K., Seppälä, J., Vestenius, M., Jalkanen, J.-P., Laakso, L., and Hakola, H.: Shipping and
607 algal emissions have a major impact on ambient air mixing ratios of non-methane hydrocarbons (NMHCs) and methanethiol
608 on Utö Island in the Baltic Sea, Atmospheric Chemistry and Physics, 24, 4717–4731, [https://doi.org/10.5194/acp-24-4717-2024](https://doi.org/10.5194/acp-24-4717-
609 2024), 2024.

610 Huffman, J. A., Docherty, K. S., Aiken, A. C., Cubison, M. J., Ulbrich, I. M., DeCarlo, P. F., Sueper, D., Jayne, J. T., Worsnop,
611 D. R., Ziemann, P. J., and Jimenez, J. L.: Chemically-resolved aerosol volatility measurements from two megacity field studies,
612 Atmos. Chem. Phys., 9, 7161–7182, <https://doi.org/10.5194/acp-9-7161-2009>, 2009.

613 Ianni, J. C.: - A comparison of the Bader-Deuflhard and the Cash-Karp Runge-Kutta integrators for the GRI-MECH 3.0 model
614 based on the chemical kinetics code Kintecus, in: Computational Fluid and Solid Mechanics 2003, edited by: Bathe, K. J.,
615 Elsevier Science Ltd, Oxford, 1368–1372, <https://doi.org/10.1016/B978-008044046-0.50335-3>, 2003.

616 Ianni, J. C.: Kintecus, 2022.

617 Jaeglé, L., Shah, V., Thornton, J. A., Lopez-Hilfiker, F. D., Lee, B. H., McDuffie, E. E., Fibiger, D., Brown, S. S., Veres, P.,
618 Sparks, T. L., Ebbin, C. J., Wooldridge, P. J., Kenagy, H. S., Cohen, R. C., Weinheimer, A. J., Campos, T. L., Montzka, D.
619 D., Digangi, J. P., Wolfe, G. M., Hanisco, T., Schroder, J. C., Campuzano-Jost, P., Day, D. A., Jimenez, J. L., Sullivan, A. P.,
620 Guo, H., and Weber, R. J.: Nitrogen Oxides Emissions, Chemistry, Deposition, and Export Over the Northeast United States
621 During the WINTER Aircraft Campaign, *Journal of Geophysical Research: Atmospheres*, 123, 12,368-12,393,
622 <https://doi.org/10.1029/2018JD029133>, 2018.

623 Ji, Y., Huey, L. G., Tanner, D. J., Lee, Y. R., Veres, P. R., Neuman, J. A., Wang, Y., and Wang, X.: A vacuum ultraviolet ion
624 source (VUV-IS) for iodide-chemical ionization mass spectrometry: a substitute for radioactive ion sources, *Atmospheric*
625 *Measurement Techniques*, 13, 3683–3696, <https://doi.org/10.5194/amt-13-3683-2020>, 2020.

626 Kercher, J. P., Riedel, T. P., and Thornton, J. A.: Chlorine activation by N_2O_5 : simultaneous, in situ detection of ClNO_2 and
627 N_2O_5 by chemical ionization mass spectrometry, *Atmospheric Measurement Techniques*, 2, 193–204,
628 <https://doi.org/10.5194/amt-2-193-2009>, 2009.

629 Le Breton, M., Hallquist, Å. M., Pathak, R. K., Simpson, D., Wang, Y., Johansson, J., Zheng, J., Yang, Y., Shang, D., Wang,
630 H., Liu, Q., Chan, C., Wang, T., Bannan, T. J., Priestley, M., Percival, C. J., Shallcross, D. E., Lu, K., Guo, S., Hu, M., and
631 Hallquist, M.: Chlorine oxidation of VOCs at a semi-rural site in Beijing: significant chlorine liberation from ClNO_2 and
632 subsequent gas- and particle-phase $\text{Cl}-\text{VOC}$ production, *Atmospheric Chemistry and Physics*, 18, 13013–13030,
633 <https://doi.org/10.5194/acp-18-13013-2018>, 2018.

634 Lee, B. H., Lopez-Hilfiker, F. D., Mohr, C., Kurtén, T., Worsnop, D. R., and Thornton, J. A.: An Iodide-Adduct High-
635 Resolution Time-of-Flight Chemical-Ionization Mass Spectrometer: Application to Atmospheric Inorganic and Organic
636 Compounds, *Environ. Sci. Technol.*, 48, 6309–6317, <https://doi.org/10.1021/es500362a>, 2014.

637 Lee, B. H., Lopez-Hilfiker, F. D., Schroder, J. C., Campuzano-Jost, P., Jimenez, J. L., McDuffie, E. E., Fibiger, D. L., Veres,
638 P. R., Brown, S. S., Campos, T. L., Weinheimer, A. J., Flocke, F. F., Norris, G., O'Mara, K., Green, J. R., Fiddler, M. N.,
639 Bililign, S., Shah, V., Jaeglé, L., and Thornton, J. A.: Airborne Observations of Reactive Inorganic Chlorine and Bromine
640 Species in the Exhaust of Coal-Fired Power Plants, *Journal of Geophysical Research: Atmospheres*, 123, 11,225–11,237,
641 <https://doi.org/10.1029/2018JD029284>, 2018a.

642 Lee, B. H., Lopez-Hilfiker, F. D., Veres, P. R., McDuffie, E. E., Fibiger, D. L., Sparks, T. L., Ebbin, C. J., Green, J. R.,
643 Schroder, J. C., Campuzano-Jost, P., Iyer, S., D'Ambro, E. L., Schobesberger, S., Brown, S. S., Wooldridge, P. J., Cohen, R.
644 C., Fiddler, M. N., Bililign, S., Jimenez, J. L., Kurtén, T., Weinheimer, A. J., Jaegle, L., and Thornton, J. A.: Flight Deployment
645 of a High-Resolution Time-of-Flight Chemical Ionization Mass Spectrometer: Observations of Reactive Halogen and Nitrogen
646 Oxide Species, *Journal of Geophysical Research: Atmospheres*, 123, 7670–7686, <https://doi.org/10.1029/2017JD028082>,
647 2018b.

648 Liao, J., Huey, L. G., Liu, Z., Tanner, D. J., Cantrell, C. A., Orlando, J. J., Flocke, F. M., Shepson, P. B., Weinheimer, A. J.,
649 Hall, S. R., Ullmann, K., Beine, H. J., Wang, Y., Ingall, E. D., Stephens, C. R., Hornbrook, R. S., Apel, E. C., Riemer, D.,
650 Fried, A., Mauldin III, R. L., Smith, J. N., Staebler, R. M., Neuman, J. A., and Nowak, J. B.: High levels of molecular chlorine
651 in the Arctic atmosphere, *Nature Geosci.*, 7, 91–94, <https://doi.org/10.1038/ngeo2046>, 2014.

652 Liu, X., Qu, H., Huey, L. G., Wang, Y., Sjostedt, S., Zeng, L., Lu, K., Wu, Y., Hu, M., Shao, M., Zhu, T., and Zhang, Y.: High
653 Levels of Daytime Molecular Chlorine and Nitryl Chloride at a Rural Site on the North China Plain, *Environ. Sci. Technol.*,
654 51, 9588–9595, <https://doi.org/10.1021/acs.est.7b03039>, 2017.

655 Macken, K. V. and Sidebottom, H. W.: The reactions of methyl radicals with chloromethanes, *International Journal of*
656 *Chemical Kinetics*, 11, 511–527, <https://doi.org/10.1002/kin.550110505>, 1979.

657 Mahmud, K., Kim, J. S., and Fontijn, A.: A high-temperature photochemical kinetics study of the oxygen atom+ hydrogen
658 chloride reaction from 350 to 1480 K, *Journal of Physical Chemistry*, 94, 2994–2998, 1990.

659 Manion, J. A., Huie, R. E., Levin, R. D., Burgess Jr., D. R., Orkin, V. L., Tsang, W., McGivern, W. S., Hudgens, J. W.,
660 Knyazev, V. D., Atkinson, D. B., Chai, E., Tereza, A. M., Lin, C.-Y., Allison, T. C., Mallard, W. G., Westley, F., Herron, J.
661 T., Hampson, R. F., and Frizzell, D. H.: NIST Chemical Kinetics Database (NIST Standard Reference Database 17, Version
662 7.0 (Web Version), Release 1.6.8, Data version 2015.09), 2015.

663 McManus, J. B., Zahniser, M. S., and Nelson, D. D.: Dual quantum cascade laser trace gas instrument with astigmatic Herriott
664 cell at high pass number, *Appl. Opt.*, 50, A74, <https://doi.org/10.1364/AO.50.000A74>, 2011.

665 McManus, J. B., Zahniser, M. S., Nelson, D. D., Shorter, J. H., Herndon, S. C., Jervis, D., Agnese, M., McGovem, R.,
666 Yacovitch, T. I., and Roscioli, J. R.: Recent progress in laser-based trace gas instruments: performance and noise analysis,
667 *Appl. Phys. B*, 119, 203–218, <https://doi.org/10.1007/s00340-015-6033-0>, 2015.

668 McNamara, S. M., Kolesar, K. R., Wang, S., Kirpes, R. M., May, N. W., Gunsch, M. J., Cook, R. D., Fuentes, J. D., Hornbrook,
669 R. S., Apel, E. C., China, S., Laskin, A., and Pratt, K. A.: Observation of Road Salt Aerosol Driving Inland Wintertime
670 Atmospheric Chlorine Chemistry, *ACS Cent. Sci.*, 6, 684–694, <https://doi.org/10.1021/acscentsci.9b00994>, 2020.

671 Mielke, L. H., Furgeson, A., and Osthoff, H. D.: Observation of ClNO₂ in a Mid-Continental Urban Environment, *Environ.*
672 *Sci. Technol.*, 45, 8889–8896, <https://doi.org/10.1021/es201955u>, 2011.

673 Moravek, A., VandenBoer, T. C., Finewax, Z., Pagonis, D., Nault, B. A., Brown, W. L., Day, D. A., Handschy, A. V., Stark,
674 H., Ziemann, P., Jimenez, J. L., de Gouw, J. A., and Young, C. J.: Reactive Chlorine Emissions from Cleaning and Reactive
675 Nitrogen Chemistry in an Indoor Athletic Facility, *Environ. Sci. Technol.*, 56, 15408–15416,
676 <https://doi.org/10.1021/acs.est.2c04622>, 2022.

677 Orlando, J. J., Tyndall, G. S., Apel, E. C., Riemer, D. D., and Paulson, S. E.: Rate coefficients and mechanisms of the reaction
678 of cl-atoms with a series of unsaturated hydrocarbons under atmospheric conditions, *International Journal of Chemical*
679 *Kinetics*, 35, 334–353, <https://doi.org/10.1002/kin.10135>, 2003.

680 Osthoff, H. D., Roberts, J. M., Ravishankara, A. R., Williams, E. J., Lerner, B. M., Sommariva, R., Bates, T. S., Coffman, D.,
681 Quinn, P. K., Dibb, J. E., Stark, H., Burkholder, J. B., Talukdar, R. K., Meagher, J., Fehsenfeld, F. C., and Brown, S. S.: High
682 levels of nitryl chloride in the polluted subtropical marine boundary layer, *Nature Geoscience*, 1, 324–328,
683 <https://doi.org/10.1038/ngeo177>, 2008.

684 Phillips, G. J., Tang, M. J., Thieser, J., Brickwedde, B., Schuster, G., Bohn, B., Lelieveld, J., and Crowley, J. N.: Significant
685 concentrations of nitryl chloride observed in rural continental Europe associated with the influence of sea salt chloride and
686 anthropogenic emissions, *Geophysical Research Letters*, 39, <https://doi.org/10.1029/2012GL051912>, 2012.

687 R Core Team: R: A language and environment for statistical computing., 2021.

688 Raff, J. D., Njegic, B., Chang, W. L., Gordon, M. S., Dabdub, D., Gerber, R. B., and Finlayson-Pitts, B. J.: Chlorine activation
689 indoors and outdoors via surface-mediated reactions of nitrogen oxides with hydrogen chloride, *Proceedings of the National*
690 *Academy of Sciences*, 106, 13647–13654, <https://doi.org/10.1073/pnas.0904195106>, 2009.

691 Riedel, T. P., Bertram, T. H., Crisp, T. A., Williams, E. J., Lerner, B. M., Vlasenko, A., Li, S.-M., Gilman, J., de Gouw, J.,
692 Bon, D. M., Wagner, N. L., Brown, S. S., and Thornton, J. A.: Nitryl Chloride and Molecular Chlorine in the Coastal Marine
693 Boundary Layer, *Environ. Sci. Technol.*, 46, 10463–10470, <https://doi.org/10.1021/es204632r>, 2012.

694 Riedel, T. P., Wagner, N. L., Dubé, W. P., Middlebrook, A. M., Young, C. J., Öztürk, F., Bahreini, R., VandenBoer, T. C.,
695 Wolfe, D. E., Williams, E. J., Roberts, J. M., Brown, S. S., and Thornton, J. A.: Chlorine activation within urban or power
696 plant plumes: Vertically resolved ClNO₂ and Cl₂ measurements from a tall tower in a polluted continental setting, *Journal of*
697 *Geophysical Research: Atmospheres*, 118, 8702–8715, <https://doi.org/10.1002/jgrd.50637>, 2013.

698 Riva, M., Pospisilova, V., Frege, C., Perrier, S., Bansal, P., Jorga, S., Sturm, P., Thornton, J. A., Rohner, U., and Lopez-
699 Hilfiker, F.: Evaluation of a reduced-pressure chemical ion reactor utilizing adduct ionization for the detection of gaseous
700 organic and inorganic species, *Atmospheric Measurement Techniques*, 17, 5887–5901, <https://doi.org/10.5194/amt-17-5887-2024>, 2024.

702 Robinson, M. A., Neuman, J. A., Huey, L. G., Roberts, J. M., Brown, S. S., and Veres, P. R.: Temperature-dependent sensitivity
703 of iodide chemical ionization mass spectrometers, *Atmospheric Measurement Techniques*, 15, 4295–4305,
704 <https://doi.org/10.5194/amt-15-4295-2022>, 2022.

705 Roscioli, J. R., Zahniser, M. S., Nelson, D. D., Herndon, S. C., and Kolb, C. E.: New Approaches to Measuring Sticky
706 Molecules: Improvement of Instrumental Response Times Using Active Passivation, *J. Phys. Chem. A*, 120, 1347–1357,
707 <https://doi.org/10.1021/acs.jpca.5b04395>, 2016.

708 Sarwar, G., Simon, H., Bhave, P., and Yarwood, G.: Examining the impact of heterogeneous nitryl chloride production on air
 709 quality across the United States, *Atmospheric Chemistry and Physics*, 12, 6455–6473, <https://doi.org/10.5194/acp-12-6455-2012>, 2012.

711 Sarwar, G., Simon, H., Xing, J., and Mathur, R.: Importance of tropospheric ClNO_2 chemistry across the Northern
 712 Hemisphere, *Geophysical Research Letters*, 41, 4050–4058, <https://doi.org/10.1002/2014GL059962>, 2014.

713 Simon, H., Kimura, Y., McGaughey, G., Allen, D. T., Brown, S. S., Osthoff, H. D., Roberts, J. M., Byun, D., and Lee, D.:
 714 Modeling the impact of ClNO_2 on ozone formation in the Houston area, *J. Geophys. Res.*, 114, D00F03,
 715 <https://doi.org/10.1029/2008JD010732>, 2009.

716 Simpson, W. R., Brown, S. S., Saiz-Lopez, A., Thornton, J. A., and von Glasow, R.: Tropospheric Halogen Chemistry:
 717 Sources, Cycling, and Impacts, *Chem. Rev.*, 115, 4035–4062, <https://doi.org/10.1021/cr5006638>, 2015.

718 Sommariva, R., Hollis, L. D. J., Sherwen, T., Baker, A. R., Ball, S. M., Bandy, B. J., Bell, T. G., Chowdhury, M. N., Cordell,
 719 R. L., Evans, M. J., Lee, J. D., Reed, C., Reeves, C. E., Roberts, J. M., Yang, M., and Monks, P. S.: Seasonal and geographical
 720 variability of nitryl chloride and its precursors in Northern Europe, *Atmospheric Science Letters*, 19, e844,
 721 <https://doi.org/10.1002/asl.844>, 2018.

722 Srinivasan, N. K., Su, M.-C., Sutherland, J. W., and Michael, J. V.: Reflected Shock Tube Studies of High-Temperature Rate
 723 Constants for $\text{OH} + \text{CH}_4 \rightarrow \text{CH}_3 + \text{H}_2\text{O}$ and $\text{CH}_3 + \text{NO}_2 \rightarrow \text{CH}_3\text{O} + \text{NO}$, *J. Phys. Chem. A*, 109, 1857–1863,
 724 <https://doi.org/10.1021/jp040679j>, 2005.

725 Tan, Z., Fuchs, H., Hofzumahaus, A., Bloss, W. J., Bohn, B., Cho, C., Hohaus, T., Holland, F., Lakshmisha, C., Liu, L., Monks,
 726 P. S., Novelli, A., Niether, D., Rohrer, F., Tillmann, R., Valkenburg, T. S. E., Vardhan, V., Kiendler-Scharr, A., Wahner, A.,
 727 and Sommariva, R.: Seasonal variation in nitryl chloride and its relation to gas-phase precursors during the JULIAC campaign
 728 in Germany, *Atmospheric Chemistry and Physics*, 22, 13137–13152, <https://doi.org/10.5194/acp-22-13137-2022>, 2022.

729 Thaler, R. D., Mielke, L. H., and Osthoff, H. D.: Quantification of Nitryl Chloride at Part Per Trillion Mixing Ratios by
 730 Thermal Dissociation Cavity Ring-Down Spectroscopy, *Anal. Chem.*, 83, 2761–2766, <https://doi.org/10.1021/ac200055z>,
 731 2011.

732 Tham, Y. J., Wang, Z., Li, Q., Yun, H., Wang, W., Wang, X., Xue, L., Lu, K., Ma, N., Bohn, B., Li, X., Kecorius, S., Größ,
 733 J., Shao, M., Wiedensohler, A., Zhang, Y., and Wang, T.: Significant concentrations of nitryl chloride sustained in the morning:
 734 investigations of the causes and impacts on ozone production in a polluted region of northern China, *Atmospheric Chemistry
 735 and Physics*, 16, 14959–14977, <https://doi.org/10.5194/acp-16-14959-2016>, 2016.

736 Tham, Y. J., Wang, Z., Li, Q., Wang, W., Wang, X., Lu, K., Ma, N., Yan, C., Kecorius, S., Wiedensohler, A., Zhang, Y., and
 737 Wang, T.: Heterogeneous N_2O_5 uptake coefficient and production yield of ClNO_2 in polluted northern China: roles of aerosol
 738 water content and chemical composition, *Atmospheric Chemistry and Physics*, 18, 13155–13171, <https://doi.org/10.5194/acp-18-13155-2018>, 2018.

740 Thornton, J. A., Kercher, J. P., Riedel, T. P., Wagner, N. L., Cozic, J., Holloway, J. S., Dubé, W. P., Wolfe, G. M., Quinn, P.
 741 K., Middlebrook, A. M., Alexander, B., and Brown, S. S.: A large atomic chlorine source inferred from mid-continental
 742 reactive nitrogen chemistry, *Nature*, 464, 271–274, <https://doi.org/10.1038/nature08905>, 2010.

743 Tripathi, N., Sahu, L. K., Patel, K., Kumar, A., and Yadav, R.: Ambient air characteristics of biogenic volatile organic
 744 compounds at a tropical evergreen forest site in Central Western Ghats of India, *J. Atmos. Chem.*, 78, 139–159,
 745 <https://doi.org/10.1007/s10874-021-09415-y>, 2021.

746 Troe, J.: Refined Representation of Falloff Curves for the Reaction $\text{HO} + \text{NO}_2 + \text{N}_2 \rightarrow (\text{HONO}_2, \text{HOONO}) + \text{N}_2$, *J. Phys.
 747 Chem. A*, 116, 6387–6393, <https://doi.org/10.1021/jp212095n>, 2012.

748 Wagner, N. L., Riedel, T. P., Young, C. J., Bahreini, R., Brock, C. A., Dubé, W. P., Kim, S., Middlebrook, A. M., Öztürk, F.,
 749 Roberts, J. M., Russo, R., Sive, B., Swarthout, R., Thornton, J. A., VandenBoer, T. C., Zhou, Y., and Brown, S. S.: N_2O_5
 750 uptake coefficients and nocturnal NO_2 removal rates determined from ambient wintertime measurements, *Journal of
 751 Geophysical Research: Atmospheres*, 118, 9331–9350, <https://doi.org/10.1002/jgrd.50653>, 2013.

752 Wallington, T., Ammann, M., Cox, R. A., Crowley, J. N., Herrmann, H., Jenkin, M. E., McNeill, V. F., Mellouki, A. W., and
 753 Troe, J.: Evaluated Kinetic Data for Atmospheric Chemistry, 2021.

754 Wang, C., Liggio, J., Wentzell, J. J. B., Jorga, S., Folkerson, A., and Abbatt, J. P. D.: Chloramines as an important
 755 photochemical source of chlorine atoms in the urban atmosphere, *Proceedings of the National Academy of Sciences*, 120,
 756 e2220889120, <https://doi.org/10.1073/pnas.2220889120>, 2023.

757 Wang, H., Yuan, B., Zheng, E., Zhang, X., Wang, J., Lu, K., Ye, C., Yang, L., Huang, S., Hu, W., Yang, S., Peng, Y., Qi, J.,
 758 Wang, S., He, X., Chen, Y., Li, T., Wang, W., Huangfu, Y., Li, X., Cai, M., Wang, X., and Shao, M.: Formation and impacts
 759 of nitrilyl chloride in Pearl River Delta, *Atmospheric Chemistry and Physics*, 22, 14837–14858, <https://doi.org/10.5194/acp-22-14837-2022>, 2022.

760 Wang, T., Tham, Y. J., Xue, L., Li, Q., Zha, Q., Wang, Z., Poon, S. C. N., Dubé, W. P., Blake, D. R., Louie, P. K. K., Luk, C.
 761 W. Y., Tsui, W., and Brown, S. S.: Observations of nitrilyl chloride and modeling its source and effect on ozone in the planetary
 762 boundary layer of southern China: ClNO_2 IN PBL OF CHINA, *J. Geophys. Res. Atmos.*, 121, 2476–2489,
 763 <https://doi.org/10.1002/2015JD024556>, 2016.

764 Wang, X., Jacob, D. J., Eastham, S. D., Sulprizio, M. P., Zhu, L., Chen, Q., Alexander, B., Sherwen, T., Evans, M. J., Lee, B.
 765 H., Haskins, J. D., Lopez-Hilfiker, F. D., Thornton, J. A., Huey, G. L., and Liao, H.: The role of chlorine in global tropospheric
 766 chemistry, *Atmospheric Chemistry and Physics*, 19, 3981–4003, <https://doi.org/10.5194/acp-19-3981-2019>, 2019.

767 Wang, X., Jacob, D. J., Downs, W., Zhai, S., Zhu, L., Shah, V., Holmes, C. D., Sherwen, T., Alexander, B., Evans, M. J., Lee, B.
 768 Eastham, S. D., Neuman, J. A., Veres, P. R., Koenig, T. K., Volkamer, R., Huey, L. G., Bannan, T. J., Percival, C. J., Lee, B.
 769 H., and Thornton, J. A.: Global tropospheric halogen (Cl, Br, I) chemistry and its impact on oxidants, *Atmospheric Chemistry
 770 and Physics*, 21, 13973–13996, <https://doi.org/10.5194/acp-21-13973-2021>, 2021.

771 Wang, Z., Wang, W., Tham, Y. J., Li, Q., Wang, H., Wen, L., Wang, X., and Wang, T.: Fast heterogeneous N_2O_5 uptake and
 772 ClNO_2 production in power plant and industrial plumes observed in the nocturnal residual layer over the North China Plain,
 773 *Atmospheric Chemistry and Physics*, 17, 12361–12378, <https://doi.org/10.5194/acp-17-12361-2017>, 2017.

774 Weissman, M. and Benson, S. W.: Heat of formation of the CHCl_2 radical. Bond dissociation energies in chloromethanes and
 775 chloroethanes, *J. Phys. Chem.*, 87, 243–244, <https://doi.org/10.1021/j100225a014>, 1983.

776 Westenberg, A. A. and deHaas, N.: Rates of $\text{H}+\text{CH}_3\text{X}$ reactions, *The Journal of Chemical Physics*, 62, 3321–3325,
 777 <https://doi.org/10.1063/1.430925>, 1975.

778 Wilkerson, J., Sayres, D. S., Smith, J. B., Allen, N., Rivero, M., Greenberg, M., Martin, T., and Anderson, J. G.: In situ
 779 observations of stratospheric HCl using three-mirror integrated cavity output spectroscopy, *Atmospheric Measurement
 780 Techniques Discussions*, 1–38, <https://doi.org/10.5194/amt-2021-6>, 2021.

781 World Meteorological Organization: Scientific Assessment of Ozone Depletion: 2022, WMO, Geneva, 2022.

782 Xia, M., Peng, X., Wang, W., Yu, C., Sun, P., Li, Y., Liu, Y., Xu, Z., Wang, Z., Xu, Z., Nie, W., Ding, A., and Wang, T.:
 783 Significant production of ClNO_2 and possible source of Cl_2 from N_2O_5 uptake at a suburban site in eastern China, *Atmospheric
 784 Chemistry and Physics*, 20, 6147–6158, <https://doi.org/10.5194/acp-20-6147-2020>, 2020.

785 Xiao, F., Sasi, P. C., Yao, B., Kubátová, A., Golovko, S. A., Golovko, M. Y., and Soli, D.: Thermal Stability and
 786 Decomposition of Perfluoroalkyl Substances on Spent Granular Activated Carbon, *Environ. Sci. Technol. Lett.*, 7, 343–350,
 787 <https://doi.org/10.1021/acs.estlett.0c00114>, 2020.

788 Ye, C., Yuan, B., Lin, Y., Wang, Z., Hu, W., Li, T., Chen, W., Wu, C., Wang, C., Huang, S., Qi, J., Wang, B., Wang, C., Song,
 789 W., Wang, X., Zheng, E., Krechmer, J. E., Ye, P., Zhang, Z., Wang, X., Worsnop, D. R., and Shao, M.: Chemical
 790 characterization of oxygenated organic compounds in the gas phase and particle phase using iodide CIMS with FIGAERO in
 791 urban air, *Atmospheric Chemistry and Physics*, 21, 8455–8478, <https://doi.org/10.5194/acp-21-8455-2021>, 2021.

792 Young, C. J., Washenfelder, R. A., Roberts, J. M., Mielke, L. H., Osthoff, H. D., Tsai, C., Pikelnaya, O., Stutz, J., Veres, P.
 793 R., Cochran, A. K., VandenBoer, T. C., Flynn, J., Grossberg, N., Haman, C. L., Lefer, B., Stark, H., Graus, M., de Gouw, J.,
 794 Gilman, J. B., Kuster, W. C., and Brown, S. S.: Vertically Resolved Measurements of Nighttime Radical Reservoirs in Los
 795 Angeles and Their Contribution to the Urban Radical Budget, *Environ. Sci. Technol.*, 46, 10965–10973,
 796 <https://doi.org/10.1021/es302206a>, 2012.

797 Yu, C., Wang, Z., Xia, M., Fu, X., Wang, W., Tham, Y. J., Chen, T., Zheng, P., Li, H., Shan, Y., Wang, X., Xue, L., Zhou, Y.,
 798 Yue, D., Ou, Y., Gao, J., Lu, K., Brown, S. S., Zhang, Y., and Wang, T.: Heterogeneous N_2O_5 reactions on atmospheric
 799

800 aerosols at four Chinese sites: improving model representation of uptake parameters, *Atmospheric Chemistry and Physics*, 20,
801 4367–4378, <https://doi.org/10.5194/acp-20-4367-2020>, 2020.

802 Zhou, W., Zhao, J., Ouyang, B., Mehra, A., Xu, W., Wang, Y., Bannan, T. J., Worrall, S. D., Priestley, M., Bacak, A., Chen,
803 Q., Xie, C., Wang, Q., Wang, J., Du, W., Zhang, Y., Ge, X., Ye, P., Lee, J. D., Fu, P., Wang, Z., Worsnop, D., Jones, R.,
804 Percival, C. J., Coe, H., and Sun, Y.: Production of N_2O_5 and ClNO_2 in summer in urban Beijing, China, *Atmospheric*
805 *Chemistry and Physics*, 18, 11581–11597, <https://doi.org/10.5194/acp-18-11581-2018>, 2018.

806